Onset of intermittent octahedral patterns in spherical Bénard convection

Philippe Beltrame, Pascal Chossat

Onset of intermittent octahedral patterns in spherical Bénard convection

Philippe Beltrame[1] and Pascal Chossat[2]

[1]Université d'Avignon - INRA, UMR1114 EMMAH, F-84914 Avignon, FRANCE
[2]laboratoire J-A Dieudonné (CNRS & Université de Nice Sophia Antipolis) Parc Valrose 06108 Nice, FRANCE

February 12, 2014

Abstract

The onset of convection for spherically invariant Rayleigh-Bénard fluid flow is driven by marginal modes associated with spherical harmonics of a certain degree ℓ, which depends upon the aspect ratio of the spherical shell. At certain critical values of the aspect ratio, marginal modes of degrees ℓ and $\ell+1$ coexist. Initially motivated by an experiment of electrophoretic convection between two concentric spheres carried in the International Space Station (GeoFlow project), we analyze the occurrence of intermittent dynamics near bifurcation in the case when marginal modes with $\ell = 3, 4$ interact. The situation is by far more complex than in the well studied $\ell = 1, 2$ mode interaction, however we show that heteroclinic cycles connecting equilibria with octahedral as well as axial symmetry can exist near bifurcation under certain conditions. Numerical simulations and continuation (using the software AUTO) on the center manifold help understanding these scenarios and show that the dynamics in these cases exhibit intermittent behaviour, even though the heteroclinic cycles may not be asymptotically stable in the usual sense.

1 Introduction

Hydrodynamical systems with a spherical symmetry can undergo complex patterns and dynamics near the onset of non uniform flow. This dynamics occurs when critical spherical modes for the linearized system, associated with spherical harmonics $Y_\ell^m(\vartheta, \varphi)$ (ℓ positive integer, $-\ell \leq m \leq +\ell$), exist with two or more different values of ℓ, hence "competing" for the instability of the trivial state [12]. In the case of the onset of thermal convection between two concentric spheres with a central gravity force, the value of ℓ is an increasing function of the aspect ratio $\eta = R_{inner}/R_{outer}$ where R_{inner} (resp. R_{outer}) is the radius length of the inner (resp. outer) boundary of the domain of convection [10]. Therefore isolated values of η exist, at which modes Y_ℓ^m ($-\ell \leq m \leq \ell$) and $Y_{\ell+1}^n$ ($-\ell+1 \leq n \leq \ell+1$) lead to instability *simultaneously*. Of course, if η is assumed close to the value 1, a larger number of modes can become unstable "almost" simultaneously. For values of η not too large (typically $\eta < 0.5$), it is relevant to consider that only two types of spherical modes, those with "degrees" ℓ and $\ell+1$, are competing for instability. Numerical calculations show that, if one assumes rigid boundary conditions, this competition occurs with $\ell = 1$ (at a critical value $\eta \simeq 0.25$), $\ell = 2$ (at $\eta \simeq 0.4$) or $\ell = 3$ (at $\eta \simeq 0.45$).

The most documented case is when $\ell = 1$. Numerical simulations by Friedrich and Haken in 1986 [23] have shown that there existed ranges of parameter values in which the dynamics for the *amplitude equations* (equations projected onto the critical modes by center manifold reduction,

1

or slaving principle) exhibited an intermittent like behaviour. It showed long periods of quasi steady states with *axisymmetric pattern* followed by sudden excursions to regimes "far" from equilibrium and relamination to another steady state similar the initial one, possibly with an axis of symmetry rotated by 90 degrees. This cycle repeats itself forever in an aperiodic manner. This case has been analysed by Chossat and Armbruster [13] who showed that under these conditions a *robust* heteroclinic cycle was bifurcating from the state of rest. A heteroclinic cycle is a set of equilibria (or other bounded solutions of a dynamical system) which are connected to each other by heteroclinic orbits in a cyclic manner. The robustness of this invariant set, which normally does not hold, can be forced by the symmetries of the system [19]. If a robust heteroclinic cycle is dynamically an attractor, then the solutions with an initial condition sufficiently close to it exhibit the intermittent behaviour described above. In a further work [18], Chossat, Guyard and Lauterbach have shown that the heteroclinic cycle occurring in this case is a "larger" object than the one described in [13], and is an attractor when the parameters of the problem belong to the range numerically explored by [23]. They called this object a *generalized* heteroclinic cycle.

Recently some interest has arisen again for onset of convection of a fluid in a spherical shell when the aspect ratio is such that spherical modes with $\ell = 3$ and 4 compete for instability. This was in relation with the preparation of the GEOFLOW experiment supported by the European Space Agency, which consists of a spherical vessel filled with a fluid subjected to an electrophoretic central force [21]. This device is placed in the International Space Station in order to simulate a self-gravitating fluid. For technical reasons the aspect ratio of the spherical shell cannot be too small and the first unstable spherical modes are expected to be of degree $\ell = 3$ or 4. Numerical simulations near onset, using a center manifold approach in the case of mode interaction, have shown flow regimes which are quite suggestive of the presence of an attracting heteroclinic cycle involving steady states with cubic and/or tetrahedral symmetries [14]. Direct simulations show the same behaviour for some time, although for the range of parameter values that have been considered, the flow seems to stabilize on a steady-state with tetrahedral symmetry after a few switches [25].

Our aim in this paper is to investigate this intermittent dynamics by analysing the bifurcation of generalized heteroclinic cycles in the case of $\ell = 3, 4$ mode interaction, in the same spirit as [13, 18]. The main ingredients of the analysis are the spherical symmetries, but also a general property of the Rayleigh-Bénard equations, namely the fact that the equations for the modes with $\ell = 4$ on the center manifold undergo a transcritical bifurcation of *unstable* steady-states (see [19]), but have a quadratic term which is relatively small and allows for a "bending back" of this branch near bifurcation [24]. It is a well-known fact that this quadratic term vanishes when the gravity force and buoyancy force follow the same law [15, 28][1]. Moreover in this case, it is also known that the signs of coefficients of quadratic terms mixing modes with degrees ℓ and $\ell + 1$ are strongly constrained and favor the occurrence of robust heteroclinic connections between pure mode steady-states.

In the experimental device, the gravity field is replaced by an electrophoretic field which has a radial dependence in r^{-5} instead of r^{-2} for the buoyancy field. Nevertheless, numerical computations of these quadratic coefficients show that in a range of physically plausible values of the Prandtl number, the above properties are still satisfied. We subsequently consider two cases: (i) gravity and buoyancy forces both having a radial dependance in r^{-2}, (ii) gravity force with radial dependence in r^{-5} with a suitably chosen Prandtl number.

It should also be noted that in [15], robust heteroclinic cycles involving steady-states with cubic (octahedral) symmetry were found to exist for values of $\ell = 8, 9$ and 13. In the present case the situation is more complex and the invariant sets which we have found involve axisymmetric

---

[1]This is a general fact when ℓ is even. The quadratic term is always 0 when ℓ is odd.

as well as cubic and, in some cases, other non axisymmetric patterns.

In Section 2 we introduce the model equations of Rayleigh-Bénard convection in a spherical shell under gravity or electrophoretic central force field, we analyze the marginal stability of the state of pure conduction, and we compute the equations on the center manifold in the case of a $\ell = 3, 4$ spherical mode interaction (subsequently called 3-4 mode interaction), with two free parameters: the deviations of Rayleigh number and aspect ratio from their critical values. In Section 3 we first recall basic facts about bifurcation in the presence of symmetry, then we describe the geometry of the 3-4 mode interaction (lattice of isotropy types). In Section 4 we analyze bifurcations and heteroclinic connections in the subspace of pure $\ell = 4$ modes. It is indeed an essential feature of this problem that $\ell = 4$ modes form an invariant submanifold of the center manifold. Moreover the equations restricted to this submanifold are gradient-like [19]. Therefore, as shown in Section 5, transverse instabilities in the $\ell = 3$ modes play a crucial role for the onset of non trivial dynamics, especially of heteroclinic cycles, even when parameters are set such that the trivial state is linearly stable along these modes. This is the case which we analyze here. The results of Sections 4 and 5 are summarized in Section 6 where the existence of heteroclinic cycles is stated. Section 7 presents a numerical exploration of the dynamics on the center manifold in the parameter range determined in previous sections. This report is concluded by a discussion on the results which have been obtained. Finally, an annex contains some material which is not immediately necessary for the understanding of this work: in Annex A the complete lattice of isotropy subgroups for the 3-4 mode interaction, in Annex B the precise form of the equivariant quadratic and cubic terms in the bifurcation equations, in Annex C the numerical scheme for the computation of the coefficients of the equations on the center manifold, in Annex D a table of eigenvalues computed at the equilibria involved in generalized heteroclinic cycles in three specific cases.

2 The model equations and their center manifold reduction for the 3-4 mode interaction

2.1 Rayleigh-Bénard convection in a spherical shell

The Rayleigh-Bénard convection is studied considering an incompressible Newtonian fluid under the Boussinesq approximation [2]. The fluid is confined between two concentric spheres of radii R_{in} and R_{out} ($R_{in} < R_{out}$). A radial force field proportional to $g(r)\mathbf{e_r}$ acts on the fluid. When the inner sphere is heated uniformly at T_{in} and the outer sphere is cooled uniformly at $T_{out} < T_{in}$ a temperature gradient $\nabla T_0(r)$ appears. For a pure diffusive state, i.e. the fluid being static, the temperature gradient is proportional to $h(r) = 1/r^2$. Due to the buoyancy force, this state may be unstable beyond a critical temperature difference leading to the convection motion. The fluid velocity $\mathbf{u}$ and the temperature perturbation $\Theta = T - T_0$ are governed by the Navier-Stokes equation and the heat transport equation. The non-dimensional equations depend on three numbers: the aspect ratio $\eta = \frac{R_{in}}{R_{out}} < 1$, the Prandtl number Pr (ratio of kinematic viscosity to thermal diffusivity) and the Rayleigh number Ra measuring the buoyancy force. The resulting equations with no-slip boundary conditions can be found in many references in literature (e.g.

[14, 5, 6]) and in our case they read after a suitable choice of scales

$$\frac{\partial \mathbf{u}}{\partial t} = -\nabla P + \Delta \mathbf{u} + \lambda g(r)\Theta \mathbf{e_r} - \mathbf{u}.\nabla \mathbf{u}, \tag{1a}$$

$$\frac{\partial \Theta}{\partial t} = Pr^{-1}\left(\Delta \Theta + \lambda h(r)\mathbf{u}.\mathbf{e_r}\right) - \mathbf{u}.\nabla \Theta \tag{1b}$$

$$\nabla.\mathbf{u} = 0, \tag{1c}$$

$$\mathbf{u}(\mathbf{r}) = \mathbf{0} \text{ for } r = \eta \text{ or } 1 \tag{1d}$$

$$\Theta(\mathbf{r}) = 0 \text{ for } r = \eta \text{ or } 1 \tag{1e}$$

where P is the pressure and the parameter λ is related to the Rayleigh number and aspect ratio by the formula

$$\lambda = \left(\frac{\eta}{1-\eta}\right)^{3/2}\sqrt{Ra}. \tag{2}$$

Using the spherical coordinates (r, ϑ, φ) the system of equations (1) is defined in the domain

$$\Omega = \{(r, \theta, \varphi) | \eta \leq r \leq 1\}. \tag{3}$$

The gravity fields $g(r)$ encountered in the geophysical context are mainly proportional to r for high-density domain (Earth's mantle) and to $1/r^2$ for low-density fluid surrounding a high density ball (like the Earth's inner core). In the laboratory, the simulated central force field can be a $1/r^5$-dependent field as for the dielectrophoretic force in the GEOFLOW experiment [9] or for a magnetic field in the dynamo experiment presented in [3]. In this work we focuse on force fields due either to gravity or dielectrophoretic effect. This latter is produced by applying an periodic high voltage ($V \simeq 10kV$) between inner and outer sphere on a dielectric fluid (silicon oil). The force acting on the volume element of the dielectric medium, consists of three parts: Coulomb force $\mathbf{F}_c = \rho_{fr}\mathbf{E}$ (ρ_{fr} free charge density), dielectrophoretic force $\mathbf{F}_d = -\frac{1}{2}\mathbf{E}^2\nabla\epsilon$ and the gradient part $\frac{1}{2}\nabla\left(\rho\frac{\partial\epsilon}{\partial\rho}\mathbf{E}^2\right)$. The last term is included in the pressure gradient ∇P in Eq. (1a). The period voltage V being much smaller than the relaxation time of free charge, the Coulomb force is neglegible. Finally the dielectrophoretic force $\mathbf{F}_d$ varies as $1/r^5$. The general theory is presented in [4] and the derivation for the GEOFLOW experiment in [7]. Note that the definition of the Rayleigh number depends on the force type:

$$Ra_g = \frac{\alpha g(R_2)}{\nu\kappa}R_2^2(T_{in} - T_{out}) : \text{gravity force} \tag{4}$$

$$Ra_e = 2\frac{\gamma\epsilon_0\epsilon_r}{\rho_0\nu\kappa}V^2(T_{in} - T_{out}) : \text{dielectrophoretic force} \tag{5}$$

The notations are as follows: α is the coefficient of volume expansion, ν the viscosity, κ the thermal conductivity and ρ_0 the density. Furthermore, ϵ_r is the dielectric constant, V the effective voltage and γ the dielectric variability. This last constant is related to the dielectric constant linear dependence on the temperature: $\epsilon = \epsilon_0\epsilon_r(1 - \gamma(T_1 - T_2))$. In the GEOFLOW experiment, the Rayleigh number Ra_e is tuned by varying the voltage V, not the temperature difference as is usually the case in planar convection experiments.

In this paper, we are interested in the dynamics close to the onset of convection as governed by the PDE's system (1) with $g(r) = r^n$, $n = -5$ or 1.

2.2 Linear stability analysis of the rest state

The linear stability of the pure conduction state $(\mathbf{u}, \Theta) = (\mathbf{0}, 0)$ in spherical symmetry has been well-studied in the case of geophysical flows since the seminal work of Chandrasekhar [2].

Because of the spherical symmetry, the eigenvalue problem is solved in irreducible representation of $\mathbf{O}(3)$ of degree ℓ. To be more precise, expressing $\mathbf{r} = (r, \vartheta, \varphi)$ and expanding the unknown fields of velocity and temperature in suitable series of spherical functions (harmonics) $Y_\ell^m(\vartheta, \varphi)$ ($-\ell \le m \le +\ell$, $\ell = 0, 1, \ldots$), the angular dependance is eliminated at each order ℓ and the eigenvalue problem reduces to solving differential boundary value problems in the r variable, of the form

$$\begin{aligned}
\mathcal{D}_\ell \mathcal{D}_\ell (ru_\ell) - \sigma u_\ell(r) &= \ell(\ell+1)\lambda g(r)\theta_\ell(r) \\
(\mathcal{D}_\ell - \sigma Pr)\theta_\ell &= -\lambda h(r) r u_\ell \\
u_\ell = \frac{d(ru_\ell)}{dr} = \theta_\ell &= 0 \ \text{ at } r = \eta, \ 1
\end{aligned}$$

where σ is the eigenvalue, u_ℓ, θ_ℓ are respectively the component of the radial velocity and the component of the temperature field along the ℓ-th spherical harmonics, and $\mathcal{D}_\ell = d/dr^2 + 2r^{-1}d/dr - \ell(\ell+1)r^{-2}$, see [2, 10] for details.

Note that, the above equations do not depend on the index m of spherical harmonics. This is a first consequence of spherical symmetry. Therefore a given solution of these equations, corresponding to a given value of ℓ, spans a $2\ell+1$ dimensional space of spherical eigenmodes associated with the same eigenvalue σ. By construction this space is an irreducible representation of $\mathbf{O}(3)$ of degree ℓ.

The eigenvalues σ are always real and they are negative when λ (or Ra) is small enough. For a given aspect ratio, the state of pure thermal conduction becomes unstable when the parameter λ exceeds the value λ_c at which the rightmost eigenvalue becomes positive. We can equivalently replace λ by the Rayleigh number Ra thanks to (2), henceforth defining a critical Rayleigh number Ra_c. The neutral stability curve for a fixed η is the set of points in the plane (ℓ, Ra) at which non trivial solutions of the eigenvalue problem exist with $\sigma = 0$. It has been shown in [10] when $g(r) = h(r) = r$ or $1/r^2$ that these curves are strictly convex. Therefore there exists a value ℓ_c at which Ra is minimal, which in turn defines the critical value Ra_c. Note that, these critical values do not depend on Pr. Numerical simulations corroborate this behavior for $g(r) = 1/r^5$ [8]. It follows that for generic values of η the critical eigenspace corresponds to an irreducible representation of degree ℓ_c, therefore it has dimension $2\ell_c + 1$. However ℓ_c depends on the aspect ratio and tends to ∞ when η tends to 1. Therefore ℓ_c is a step function of η and at the boundaries of the intervals so defined, two different critical degrees ℓ_c and $\ell_c + 1$ coexist. These values η_c define in the (η, Ra) plane, codimension 2 bifurcation points with ℓ_c, ℓ_c+1 mode interaction.

This is illustrated by the figure 2.2 below, which shows numerical results on the computation of the neutral stability curve in the plane (η, Ra) for different values of ℓ. The critical Ra_c and ℓ_c are defined by the lower enveloppe of the curves and the codimension 2 bifurcation points are the points on the enveloppe at which two curves intersect.

In the rest of this paper we concentrate on the $3, 4$ mode interaction, which in both cases $g(r) = 1/r^2$ and $g(r) = 1/r^5$ correspond to a critical $\eta_c \sim 0.45$. The corresponding critical eigenspace V has therefore dimension 16.

In the following we define V^k to be the space of spherical harmonics of degree $\ell = k$, so that $V = V^3 \oplus V^4$.

2.3 Center manifold reduction for the 3-4 mode interaction

The onset of convection can be examined by varying the two parameters $\tilde{\lambda} = \lambda - \lambda_c$ and $\tilde{\eta} = \eta - \eta_c$. The system (1) defined in a suitable Hilbert space verifies the assumption of the center manifold theorem [17]. Therefore, the dynamics near the onset is governed by an ODE
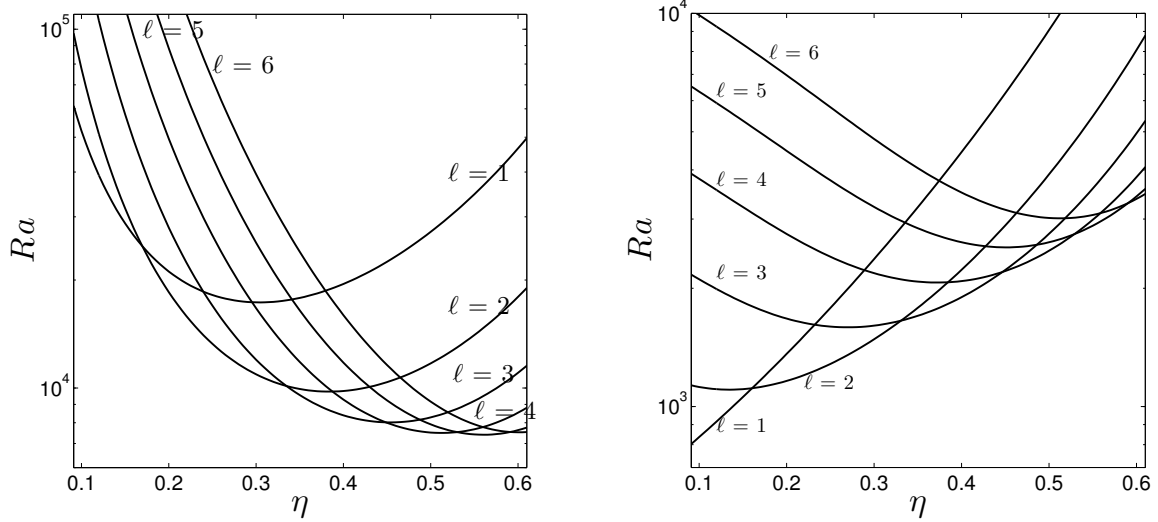
Figure 1: Neutral stability curves in the cases $g(r) = 1/r^2$ (left) and $g(r) = 1/r^5$ (right) for values of ℓ up to 6. For a given η, the lowest point gives the critical values of Ra and ℓ.
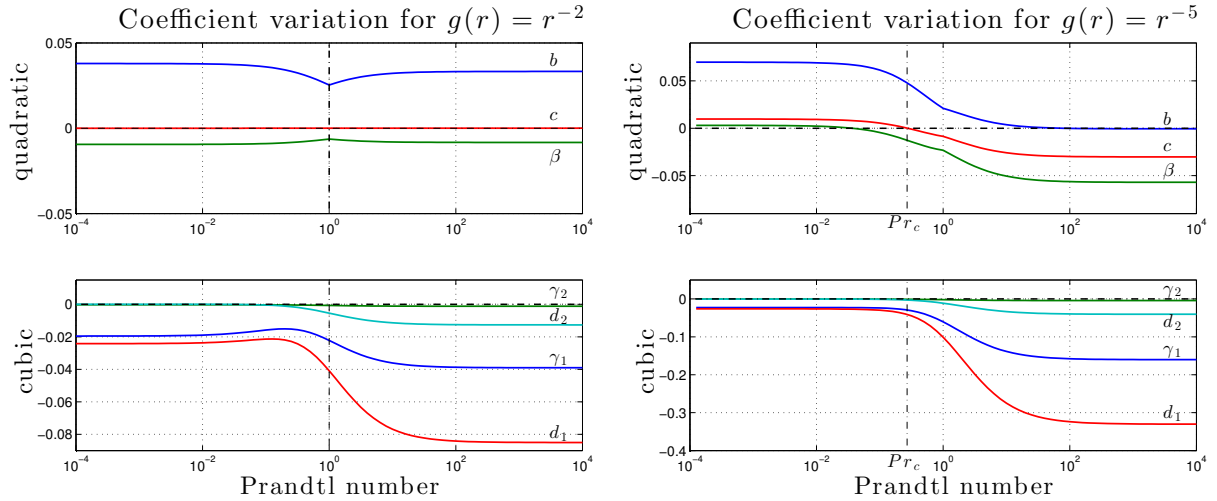
Figure 2: Quadractic and cubic coefficients in Equations (9) as functions of the Prandtl number. Left: case $g(r) = 1/r^2$, right: case $g(r) = 1/r^5$. Pr_c indicates the critical value vanishing c for $g(r) = r^{-5}$.

system of the size of the critical eigenspace. Our theoretical and numerical analysis focuses on that 16-dimensional ODE' system. The reduction on the center manifold is provided in [15, 8] in the Rayleigh-Bénard convection framework. We outline the main steps and refer to [15, 8] for details.

First, write (1) as an evolution problem for the field $Z(t) = (\mathbf{u}(t), \Theta(t))$ in a suitable Hilbert space setting (see above references):

$$\frac{\partial Z}{\partial t} = F(Z, \tilde{\lambda}, \tilde{\eta}) \tag{6a}$$

$$= L_0 Z + \tilde{\lambda} L_1 Z + \tilde{\eta} L_2 Z + 0(\tilde{\eta}^2) L_3 Z + M(Z, Z). \tag{6b}$$

L_0 is the Jacobian matrix of F at the critical point, L_1 and L_2 are the linear perturbations of L_0 of order respectively $\tilde{\lambda}$ and $\tilde{\eta}$. L_3 is the remaining linear operator containing the $O(\tilde{\eta}^2)$ terms, which can be neglected in the bifurcation analysis. The bilinear operator M is symmetric and is defined in [15].

In a second step the evolution equation (6) is decomposed along the projection P_0 on the kernel of L_0 which commutes with L_0 and its complement $1 - P_0$. Here from Section 2.2, V is the space of critical spherical modes with $\ell = 3$ and 4. According to the center manifold theorem any solution Z of Eq. (6) in a neighborhood of $(Z, \tilde{\lambda}, \tilde{\eta}) = (0, 0, 0)$ can be decomposed as follows: $Z(t) = X(t) + Y(X, \tilde{\lambda}, \tilde{\eta}, t)$, where $X = P_0 Z$ and $Y = (1 - P_0)Z$. Then the problem (6) takes the form

$$
\begin{aligned}
\dot{X} &= P_0 F(X + Y, \tilde{\lambda}, \tilde{\eta}) \\
\dot{Y} &= (I - P_0) F(X + Y, \tilde{\lambda}, \tilde{\eta}).
\end{aligned}
\tag{7}
$$

To solve these equations one expands $Y(X, \tilde{\lambda}, \tilde{\eta})$ in power series, the second equation can be then solved recursively at each power starting from the lowest order, so that the first equation gives a polynomial approximation of the equation on the center manifold:

$$
\dot{X} = \sum_{pqr} \tilde{\lambda}^q \tilde{\eta}^r R_{qr}^p(X, ..., X),
\tag{8}
$$

where R_{qr}^p is p-linear and symmetric. This *bifurcation equation* is therefore a 16 dimensional system of ODE's.

The third step consists in performing the actual computation of the R_{qr}'s. By taking the coordinates of X along the spherical harmonics Y_3^j and Y_4^k, we can set $X = [(x_{-3}, \cdots, x_3), (y_{-4}, \cdots, y_4)]$. Note that, since X is real, the coordinates verify $x_{-m} = (-1)^m \overline{x}_m$ and $y_{-n} = (-1)^n \overline{y}_n$. It is essential here to know that the series expansion (8) keeps the $O(3)$ symmetry. In other words if T_g denotes the action of $g \in O(3)$ in V, then $R_{qr}^p(T_g X, ..., T_g X) = T_g R_{qr}^p(X, ..., X)$. This property leads to a substantial simplification of the expression of these terms, many of them being actually identically equal to 0. Calculations which we do not detail here show that the leading part of the equations finally read

$$
\begin{aligned}
\dot{x}_j &= \mu_1 x_j + \beta Q_j^{(1)}(x_{-3}, \cdots, x_3, y_{-4}, \cdots, y_4) + \gamma_1 \|(x_{-3}, \cdots, x_3)\|^2 x_j \\
&\qquad\qquad\qquad\qquad + \gamma_2 C_j^{(1)}(x_{-3}, \cdots, x_3)
\end{aligned}
\tag{9a}
$$

$$
\begin{aligned}
\dot{y}_k &= \mu_2 y_k + b Q_k^{(2)}(x_{-3}, \cdots, x_3) + c Q_k^{(3)}(y_{-4}, \cdots, y_4) + d_1 \|(y_{-4}, \cdots, y_4)\|^2 y_k \\
&\qquad\qquad\qquad\qquad + d_2 C_k^{(2)}(y_{-4}, \cdots, y_4)
\end{aligned}
\tag{9b}
$$

where the quadratic Q's and cubic C's are expressed in B.

The norm of $X \in V$ is defined as follows:

$$
\|X\|^2 = \sum_{-3}^{3} (-1)^k x_k x_{-k} + \sum_{-4}^{4} (-1)^m y_m y_{-m}.
$$

The two sums correspond respectively to the square of the norm in the $\ell = 3$ modes and to the square of the norm in the $\ell + 1 = 4$ modes. Note that the subspace of "pure" 4 modes is flow-invariant (this is a consequence of properties of isotropy subgroups for the action of $O(3)$ in V, which we shall recall in the next section).

The coefficients in front of these polynomial terms depend on the physical parameters and in particular, on the Prandtl number. Using the inductive algorithm presented in [15] the coefficients are expressed in C and computed order by order for various Prandtl numbers. The results for $g = 1/r^5$ can be found in [16]. They are gathered in Fig. 2.3 for both force fields.

According to [23, 16] when $Pr > 1$, time and unknowns are changed as follows: time is multiplied by Pr and X is divided by $\sqrt{Pr}$. It results that the quadratic coefficient are divided by $\sqrt{Pr}$.

In the case $g(r) = 1/r^2$, the results agree with the following properties, which were proved in a more general context in [12], independantly of the value of Pr:

1. $c = 0$

2. $b = -2\beta$

3. $\gamma_1 < 0$ and $d_2 < 0$.

The proof is based on the fact that L_0 is a self-adjoint operator when $g(r) = 1/r^2$.
Moreover we also see from Fig. 2.3 that $d_1 < d_2 < 0$ for all Pr.
In the case $g(r) = 1/r^5$, equalities (i) and (ii) are nearly satisfied if Pr is equal to a critical value $Pr_c \simeq 0.27$, despite the fact that L_0 is no longer self-adjoint. Moreover all the above inequalities are also true in this case. These properties of the coefficients will play an important role in our bifurcation and stability analysis.
The condition $c = 0$ introduces an additional degeneracy in the bifurcation problem, as we shall see in Section 4. Assuming either that the force field $g(r)$ is slightly perturbed from $g(r) = 1/r^2$, or in the case $g(r) = 1/r^5$, that Pr is close to Pr_c, we can consider the coefficient c to be an additional parameter close to 0.

Remark that $\beta < 0$ when $g(r) = 1/r^2$ and also when $g(r) = 1/r^5$, near the critical Pr_c. Changing the time scale we can always assume $\beta = -1$, which we shall do in the subsequent analysis.

3 Basic facts about bifurcation with symmetry and the isotropy lattice

3.1 Basic facts about equivariant bifurcation theory

Because symmetry is responsible for the high dimension of the center manifold while its geometry is by no way simple, the use of concepts and techniques of Equivariant Bifurcation Theory [26, 20] will be of crucial importance in the forthcoming bifurcation analysis. We introduce first some general and basic facts, then in the next subsection we describe the geometry of the action of $\mathbf{O}(3)$ on the center manifold, and in the last subsection we apply these informations to describe the elementary bifurcations which occur in this problem.

We denote by $T(g)$, $g \in G$, the representation of the group $G = \mathbf{O}(3)$ in the space V. In other words T is a homomorphism from G to $GL(V)$ (the linear group of all invertible linear maps in V).

Definition 1 *(i) Given $x \in V$, the set $G_x = \{g \in G \ / \ T(g)x = x\}$ is the* isotropy subgroup *of x.*
(ii) Given an isotropy subgroup H, the linear space $Fix(H) = \{x \in X \ / \ T(H)x = x\}$ is the fixed-point subspace *associated with H. If $\dim Fix(H) = 1$, one often call it an* axis of symmetry *for the action of G in V.*
(iii) Given a point $x \in V$, the set $\mathcal{O}_x = \{T(g)x \ / \ g \in G\}$ is the G-orbit of x.

The three following statements are elementary: (i) If $H \subset H'$ are two isotropy subgroups, then $Fix(H) \supset Fix(H')$.
(ii) The largest subgroup of G, which leaves $Fix(H)$ invariant is its normalizer $N(H)$[2].

---

[2]The normalizer of H is the group of elements g in G such that $gHg^{-1} = H$.

(iii) Two points in the same G-orbit have conjugated isotropy subgroups.
In fact the G-orbit of a point is a compact manifold whose dimension is given by

$$\dim O_x = \dim G - \dim G_x \qquad (10)$$

Since here $\dim G = 3$ and $\dim G_x$ can be either 0 (case of a finite isotropy subgroup), 1 or 3, $\dim \mathcal{O}_x$ can be either 3, 2 or 0. We can classify G-orbits by conjugacy classes of isotropy subgroups. These conjugacy classes are called *isotropy types* or *orbit types* and they are partially ordered by group inclusion. This ordering is called the *lattice* of isotropies of the group action.

The knowledge of the lattice of isotropy types is useful in the study of dynamical systems with symmetry for the following reason [20]. Consider a G-equivariant differential equation in a space V, like Eq. (9). Then any fixed-point subspace is invariant by this equation. As a consequence, if the initial condition belongs to a subspace $Fix(H)$, then the whole trajectory lies in $Fix(H)$. In fact, the subset of points which have exactly isotropy H is flow-invariant. This subset is open in $Fix(H)$ and its boundary is filled with points with higher isotropy.
Symmetry has another general consequence. Suppose that the action of G in V does not contain the trivial representation, as in our $3-4$ mode interaction. Then $x = 0$ is a solution for all parameter values. Indeed writing the bifurcation equation $F(x, \mu) = 0$, we have by equivariance $T(g)F(0, \mu) = F(0, \mu)$, but since V does not contain the trivial representation only 0 is fixed by $T(g)$ for all g.
These two remarks put together allow to state a general bifurcation result in systems with symmetry, known as the Equivariant Branching Lemma [26]. We give here a version of the lemma suitable to our purpose. Note that, if $Fix(H)$ is an axis of symmetry, $N(H)$ can act on $Fix(H)$ either trivially or by $x \mapsto \pm x$. As above we assume the action of G in V does not contain the trivial representation.

Lemma 1 *Let H be an isotropy subgroup with $\dim Fix(H) = 1$. Let $f(x, \mu) = 0$ be the bifurcation equation restricted to $Fix(H)$, $f \in \mathcal{C}^k(\mathbb{R} \times \mathbb{R}^m, \mathbb{R})$, $k > 2$, such that $f'_x(0,0) = 0$ (bifurcation condition). Then*
(i) if $N(H)$ acts trivially on $Fix(H)$, $f''_{x\mu}(0,0) \neq 0$ and $f''_{x^2}(0,0) \neq 0$, a transcritical branch of solutions with isotropy H bifurcates from 0;
(ii) if $N(H)$ acts by $\pm Id$ in $Fix(H)$, $f''_{x\mu}(0,0) \neq 0$ and $f'''_{x^3}(0,0) \neq 0$, a pitchfork branch of solutions bifurcates from 0.

Note that, the conditions on the derivatives of f are "generic" in each of cases (i) and (ii), which loosely means that they should be only exceptionally wrong. However in case (i), as we have already seen in Section 2.3, the condition $f''_{x^2}(0,0) \neq 0$ can be unsatisfied in certain cases in Rayleigh-Bénard convection. This point will be of crucial importance in all our bifurcation analysis.
Of course bifurcated solutions with lower isotropy may also exist, but there is no such simple statement as the above lemma.
As we shall see, symmetry affects not only the bifurcation of steady-states but also the type of dynamics that can exist.

3.2 The isotropy lattice and fixed-point subspaces

We have listed all isotropy types and determined representative fixed-point subspaces by exploiting the informations provided in [20] (Appendix A). The lattice of isotropies is a quite complicated graph, which we show in A. Table 1 contains the relevant informations for isotropy types with fixed-point subspace of dimension lower that 6. These are the most relevant for our

purpose. As above (Section 2.3) we note $(x_{-3}, \cdots, x_3)$ for the component along the $\ell = 3$ spherical harmonics Y_3^j, and $(y_{-4}, \cdots, y_4)$ for the component along the $\ell = 4$ spherical harmonics Y_4^k. Note that, $Y_\ell^{-m} = (-1)^m \overline{Y}_\ell^m$ and therefore the same holds for the coordinates (real space). Also note that the antipodal symmetry $S : \mathbf{r} \mapsto -\mathbf{r}$ acts as $-Id$ on spherical harmonics with odd degree ℓ, while it acts trivially on spherical harmonics with even degree. It follows that the group $\mathbb{Z}_2^c = \{Id, S\}$ is an isotropy subgroup whose fixed-point subspace is 9 dimensional and consists of all the spherical modes with $\ell = 4$ (irreducible representation of degree 4). We shall note $V^4 = Fix(\mathbb{Z}_2^c)$. The notations of groups in table 1 are taken from [26]. These groups are

Isotropy H	$Fix(H)$	Isotropy H	$Fix(H)$
$\mathbf{O}(2) \oplus \mathbb{Z}_2^c$	y_0	$\mathbf{D}_2 \oplus \mathbb{Z}_2^c$	(y_0, y_{2r}, y_{4r})
$\mathbb{O} \oplus \mathbb{Z}_2^c$	$y_{4r} = \pm \eta y_0$	$\mathbf{D}_4^d$	(x_{2i}, y_0, y_{4r})
$\mathbf{O}(2)^-$	(x_0, y_0)	$\mathbf{D}_3$	(x_{3i}, y_0, y_{3r})
$\mathbf{D}_4 \oplus \mathbb{Z}_2^c$	(y_0, y_{4r})	$\mathbf{D}_2$	$(x_{2i}, y_0, y_{2r}, y_{4r})$
$\mathbf{D}_6^d$	(x_{3r}, y_0)	$\mathbf{D}_3^z$	$(x_0, x_{3r}, y_0, y_{3r})$
$\mathbf{D}_3 \oplus \mathbb{Z}_2^c$	(y_0, y_{3r})	$\mathbf{D}_2^z$	$(x_0, x_{2r}, y_0, y_{2r}, y_{4r})$
$\mathbb{O}^-$	$(x_{2i}, y_{4r} = \eta y_0)$	$\mathbb{Z}_2 \oplus \mathbb{Z}_2^c$	$(y_0, y_2, \bar{y}_2, y_4, \bar{y}_4)$
$\mathbf{D}_4^z$	(x_0, y_0, y_{4r})	$\mathbb{Z}_4^-$	$(x_2, \bar{x}_2, y_0, y_4, \bar{y}_4)$

Table 1: Fixed-point subspaces for representatives of the isotropy types such that $\dim Fix(H) \leq 5$. We have noted $\eta = \sqrt{\frac{5}{14}}$. Another useful representation of $Fix(\mathbb{O} \oplus \mathbb{Z}_2^c)$ is $y_{3r} = \nu y_0$ with $\nu = \sqrt{\frac{10}{7}}$.

defined as follows (up to conjugacy).
- $\mathbf{D}_n$ is the group generated by the n-fold rotation R_n about an axis δ (which we choose as the vertical z-axis) and rotation by π around an axis perpendicular to δ (noted χ). This group is isomorphic to the dihedral group of order $2n$. Note that χ acts in V as follows: $\chi \cdot x_j = -\bar{x}_j$, $\chi \cdot y_k = \bar{y}_k$. $\mathbf{D}_n \oplus \mathbb{Z}_2^c$ is then the full group of symmetry of a prism with regular n-gon basis (the notation $\oplus$ means "direct product"). Similarly, $\mathbf{O}(2) \oplus \mathbb{Z}_2^c$ is the full symmetry group of a cylinder.
- $\mathbb{O}$ is the group of direct (rotational) symmetries of a cube or octahedron. Hence $\mathbb{O} \oplus \mathbb{Z}_2^c$ is the full symmetry group of a cube.
- Let K be the reflection through a plane containing δ. Then $\mathbf{D}_n^z$ is the group generated by R_n and K. This group is isomorphic to $\mathbf{D}_n$. Similarly, $\mathbf{D}_{2n}^d$ is the group generated by $\mathbf{D}_n$ and K. It contains $4n$ elements.
- $\mathbb{O}^-$ is the group generated by the tetrahedral group $\mathbb{T}$ (group of direct symmetries of a tetrahedron) and by K (here δ is the axis of a 3-fold rotation in $\mathbb{T}$). This group contains 24 elements and is isomorphic to the octahedral group $\mathbb{O}$.
- Let $K_\perp$ be the reflection through the plane orthogonal to δ. Then $\mathbb{Z}_{2n}^-$ ($n > 1$) is the group generated by the transformation KR_{2n} (it is cyclic of order $2n$). $\mathbb{Z}_2^-$ is the 2-element group generated by any reflection through a plane. The reflection κ through $K_\perp$ acts as follows in V: $\kappa \cdot x_j = (-1)^{j+1} x_j$, $\kappa \cdot y_k = (-1)^k y_k$.

Note that, all isotropy subgroups which do not contain $\mathbb{Z}_2^c$ have fixed-point subspaces which contain $\ell = 3$ modes. We call these subspaces *mixed mode subspaces*.

4 Bifurcation with pure $\ell = 4$ modes

We have seen that the subspace V^4 of pure $\ell = 4$ modes is also the subspace of points which are fixed by the antipodal symmetry, therefore it is flow-invariant. The bifurcation problem with $\ell = 4$ has been completely resolved in the "generic", codimension 1 case in [19].

By Table 3.2, two isotropy types have axes of symmetry: $\mathbf{O}(2) \oplus \mathbb{Z}_2^c$ and $\mathbb{O} \oplus \mathbb{Z}_2^c$. Solutions with the former isotropy are axisymmetric and those with the latter isotropy have octahedral (cubic) symmetry. Both solutions are also invariant by reflections through the equatorial plane.

According to Lemma 1, the bifurcated branches should be transcritical since $N(H \oplus \mathbb{Z}_2^c) = H \oplus \mathbb{Z}_2^c$ when $H = \mathbf{O}(2)$ and $\mathbb{O}$. However we have also seen in Section 2.3 that the quadratic terms of the equations restricted to the pure $\ell = 4$ modes vanish when $g(r) = r^{-2}$, or, in the case when $g(r) = r^{-5}$, if the Prandtl number is close to a critical value Pr_c. This leads to a codimension 2 bifurcation problem, which has been studied from a singularity theory point of view in [24], then applied to the spherical Bénard problem in [28] (with different force field and boundary conditions).

The subsequent analysis can be put into this perspective: the coefficient c of the "pure" quadratic terms is now considered a *free parameter close to 0*, and we further assume $c > 0$. Indeed according to [24], the case $c < 0$ leads to more complicated bifurcation diagrams in V^4 and hardly identifiable heteroclinic cycles.

Next we provide useful material for the further dynamical analysis. First we compute the primary branches of steady-states and their stability, then we study the bifurcation diagrams in the invariant plane $Fix(\mathbf{D}_4 \oplus \mathbb{Z}_2^c)$, finally we state a proposition about the bifurcation diagram in V^4.

4.1 The axisymmetric equilibria.

On the axis $Fix(\mathbf{O}(2) \oplus \mathbb{Z}_2^c)$ the (scalar) bifurcation equation reads

$$0 = \mu_2 y_0 + 9cy_0^2 + (d_1 + d_2)y_0^3.$$

where μ_2 is the bifurcation parameter. It follows that the bifurcated equilibria satisfy the relation

$$\mu_2 = -9cy_0 - (d_1 + d_2)y_0^2 \tag{11}$$

A turning point exists at $y_0 = -\frac{9c}{2(d_1+d_2)}$ and since $d_1 + d_2 < 0$ (for any value of Pr) the parabola is always oriented towards $y_0 > 0$.

Even in the limit $c = 0$, the two branches of the parabola correspond to symmetrically distinct states. We denote by $\alpha_\pm$ these branches. According to (10), the corresponding $\mathbf{O}(3)$-orbits of equilibria have dimension 2.

In order to determine their stable and unstable manifolds in V we need to compute the eigenvalues of the Jacobian matrix $L_{\alpha_\pm}$ of the vector field linearized at $\alpha_\pm$, hence to determine first the isotypic decomposition of the action of $\mathbf{O}(2) \oplus \mathbb{Z}_2^c$ in the $3, 4$ representation of $\mathbf{O}(3)$ [20]. A straightforward (and classical) analysis shows that $L_{\alpha_\pm}$ decomposes into two 1×1 and seven 2×2 diagonal blocks along the coordinates x_0, y_0, $(x_j, \bar{x}_j)$ $(j = 1, 2, 3)$ and $(y_m, \bar{y}_m)$ $(m = 1, 2, 3, 4)$ respectively. The block in the $(y_1, \bar{y}_1)$ subspace is the 0 matrix, corresponding to the fact that this plane is tangent to the $\mathbf{O}(3)$ orbit of $\alpha_\pm$ [19]. The other eigenvalues are listed in the following table 2 where y_0 is the coordinate of $\alpha_\pm$.

4.2 The octahedral equilibria.

We now turn to the bifurcations along the axis $Fix(\mathbb{O} \oplus \mathbb{Z}_2{}^c)$ defined by the relation $y_{4r} = \sqrt{5/14}y_0$. The bifurcation equation along this axis, which we parametrize with y_0, reads

$$0 = \mu_2 y_0 + 14cy_0^2 + (\frac{12}{7}d_1 - \frac{16}{49}d_2)y_0^3$$

Eigenvalues	Multiplicity	Eigenspaces
$\sigma_0^\alpha = \mu_1 - 6y_0$	1	x_0
$\sigma_1^\alpha = \mu_1 - y_0$	2	$\{x_1, \bar{x}_1\}$
$\sigma_2^\alpha = \mu_1 + 7y_0$	2	$\{x_2, \bar{x}_2\}$
$\sigma_3^\alpha = \mu_1 - 3y_0$	2	$\{x_3, \bar{x}_3\}$
$\lambda_0^\alpha = 9cy_0 + (2d_1 + d_2)y_0^2$	1	y_0
$\lambda_1^\alpha = 0$	2	$\{y_1, \bar{y}_1\}$
$\lambda_2^\alpha = -20cy_0 + 5/2 d_2 y_0^2$	2	$\{y_2, \bar{y}_2\}$
$\lambda_3^\alpha = -30cy_0 - 45/28 d_2 y_0^2$	2	$\{y_3, \bar{y}_3\}$
$\lambda_4^\alpha = 5cy_0 - 20/7 d_2 y_0^2$	2	$\{y_4, \bar{y}_4\}$

Table 2: Eigenvalues of the linearized vector field at $\alpha = \alpha_\pm$

and therefore the bifurcated branches are given by

$$\mu_2 = -14cy_0 - Dy_0^2 \quad \text{where } D = 12/7 d_1 - 16/49 d_2 \tag{12}$$

Since $d_1 < d_2 < 0$ (Fig. 2.3), $D < 0$ and the parabola is oriented towards $y_0 > 0$. Here again the two branches correspond to symmetrically distinct states.

We note these solutions β_+ and β_-. They generate three-dimensional $\mathbf{O}(3)$-orbits of equilibria. The eigenvalues of the Jacobian matrix $L_{\beta_\pm}$ of the vector field linearized at $\beta_\pm$ are listed in the following table 3, together with the corresponding eigenspaces. Here again the multiplicity and eigenspaces result from the isotypic decomposition of the action of $\mathbb{O} \oplus \mathbb{Z}_2{}^c$ in the $\ell = 3, 4$ representation of $\mathbf{O}(3)$. The convention is that coordinates which do not appear in the definition of eigenspaces must be set equal to 0. The $\beta_\pm$ solutions are parametrized by the coordinate y_0.

Eigenvalues	Multiplicity	Eigenspaces
$\sigma_0^\beta = \mu_1 + 12y_0$	1	$\{x_{2i}\}$
$\sigma_1^\beta = \mu_1 - 6y_0$	3	$\{x_0, x_3 = -\frac{\sqrt{15}}{3}\bar{x}_1\}$
$\sigma_2^\beta = \mu_1 + 2y_0$	3	$\{x_{2r}, x_3 = \frac{\sqrt{15}}{5}\bar{x}_1\}$
$\lambda_0^\beta = 14cy_0 + (24/7 d_1 - 32/49 d_2)y_0^2$	1	$\{y_{4r} = \sqrt{\frac{5}{14}}y_0)$
$\lambda_1^\beta = 0$	3	$(y_{4i}, y_3 = -\frac{\sqrt{7}}{7}\bar{y}_1)\}$
$\lambda_2^\beta = -10cy_0 + 40/7 d_2 y_0^2$	2	$\{y_{2r}, y_{4r} = -\sqrt{\frac{7}{10}}y_0\}$
$\lambda_3^\beta = -40cy_0 + 10/7 d_2 y_0^2$	3	$\{y_{2i}, y_3 = \sqrt{7}\bar{y}_1\}$

Table 3: Eigenvalues of the linearized vector field at $\beta = \beta_\pm$

4.3 Bifurcation in the invariant planes.

There are two types of fixed-point planes in V^4, with representatives

$$P = Fix(\mathbf{D}_4 \oplus \mathbb{Z}_2{}^c) = \{y_0, y_{4r}\}$$
$$P_1 = Fix(\mathbf{D}_3 \oplus \mathbb{Z}_2{}^c) = \{y_0, y_{3r}\}.$$

Each of them contains the axis $Fix(\mathbf{O}(2) \oplus \mathbb{Z}_2{}^c) = \{y_0\}$ and two copies of the axes of cubic isotropy $\mathbb{O} \oplus \mathbb{Z}_2{}^c$: namely $\{y_{4r} = \pm\sqrt{5/14}y_0\}$ in P, and $\{y_{3r} = \pm\sqrt{10/7}y_0\}$ in P_1.

We focus on the plane P. The case of P_1 would be treated similarly and we just indicate the result. Writing $u = y_0$ and $v = y_{4r}$ to simplify notations, the equations in P read

$$\dot{u} = \mu_2 u + c(9u^2 + 14v^2) + d_1 u(u^2 + 2v^2) + d_2 u(u^2 - \tfrac{26}{7}v^2)$$
$$\dot{v} = \mu_2 v + 14cuv + d_1 v(u^2 + 2v^2) + d_2 v(-\tfrac{13}{7}u^2 + \tfrac{30}{7}v^2)$$

We note $\beta_\pm$, resp. $\tilde{\beta}_\pm$, the equilibria satisfying $y_{4r} = \eta y_0$, resp. $y_{4r} = -\eta y_0$. β_+ and $\tilde{\beta}_+$ are exchanged by rotation $\phi = \pi/4$, idem for β_- and $\tilde{\beta}_-$. Equilibria off the invariant axes must

12

satisfy the conditions $u = \frac{7c}{4d_2}$ and $\mu_2 = -\frac{7c^2}{16d_2^2}(7d_1 + 43d_2) - (2d_1 + \frac{30}{7}d_2)v^2$. We see that a secondary bifurcation off the α branch occurs at

$$\mu_2^\alpha = -(7d_1 + 43d_2)\frac{7c^2}{16d_2^2} \tag{13}$$

This branch is a supercritical *pitchfork*. If $c > 0$ the branching occurs from an α_- equilibrium. It corresponds to a change of sign of the eigenvalue λ_4^α (Table 2).

Let us denote by γ, $\tilde{\gamma}$ these equilibria with isotropy $\mathbf{D}_4 \oplus \mathbb{Z}_2{}^c$. As μ_2 is increased, they move closer to the invariant axes with cubic isotropy until they cross them at the value

$$\mu_2^\beta = -(21d_1 + 94d_2)\frac{c^2}{4d_2^2}. \tag{14}$$

Observe that one always have $\mu_2^\alpha < \mu_2^\beta$. This value μ_2^β corresponds to a *transcritical* bifurcation from β and $\tilde{\beta}$ solutions. When $c > 0$, these secondary bifurcations correspond to the change of sign of the eigenvalue $\lambda_2^{\beta_-}$ (see Table 3).

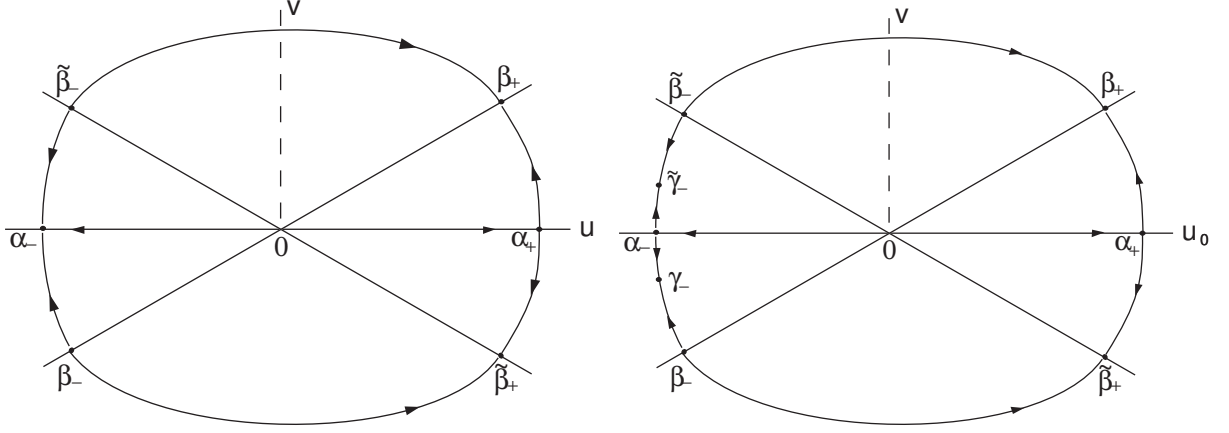The phase diagram in P when $0 < \mu_2 < \mu_2^\beta$ looks like in Fig. 3. Observe that as long as

Figure 3: Sketch of the phase portrait in $P = Fix(\mathbf{D}_4 \oplus \mathbb{Z}_2{}^c)$. Left: $0 < \mu_2 < \mu_2^\alpha$, right: $\mu_2^\alpha < \mu_2 < \mu_2^\beta$.

$\mu_2 < \mu_2^\alpha$, saddle-sink heteroclinic orbits connect the α_- to the β_- equilibria in P.

When $\mu > \mu_2^\beta$, γ passes on the other side of the β axis and the connections between α_- and β_- equilibria are restored but the arrows are reversed.

In the plane P_1, same calculations show that as long as μ_2 is smaller than $\hat{\mu}_2^\alpha = -8(168d_1 + 17d_2)c^2/d_2$ the phase diagram looks like Fig. 3 (left), except that the β and $\tilde{\beta}$ axes are reversed and α_+ is stable while α_- is unstable. Note that, $\hat{\mu}_2^\alpha > \mu_2^\beta$.

4.4 Bifurcation off the invariant planes in V^4

A complete description of the bifurcations with parameters μ_2 and c in V^4 was made in [24] and we rely on their results. The system is 3-determined and the equations restricted to order 3 are gradient, which implies that no non trivial dynamics exists in a neighborhood of the bifurcation. We need however to making precise statements about heteroclinic connections between equilibria in V^4.

Proposition 1 *Suppose $\mu_2 > 0$ and $c > 0$ is close enough to 0. Then*

13

(i) *A flow-invariant and attracting topological sphere exists in V^4, which contains all the bifurcated equilibria.*

(ii) *The $\mathbf{O}(3)$ orbit of octahedral equilibria β_+ is attracting. The other branches of equilibria have types β_- and $\alpha_\pm$. If $\mu_2 > \mu_2^\alpha$, a secondary branch γ with isotropy $\mathbf{D}_4 \oplus \mathbb{Z}_2{}^c$ bifurcates from α_- and crosses the branch β_- when μ_2 crosses μ_2^β. There are no other bifurcated equilibria when μ_2 is smaller than a critical value which is greater that μ_2^β.*

(iii) *The robust heteroclinic connections between these orbits of equilibria are sketched in Fig. 4. The numbers indicate the dimensions of the manifolds of connections in the unstable manifolds of the equilibria at the base of the arrows. Remaining dimensions (recall that $\dim V^4 = 9$) correspond to stable submanifolds of the equilibria.*
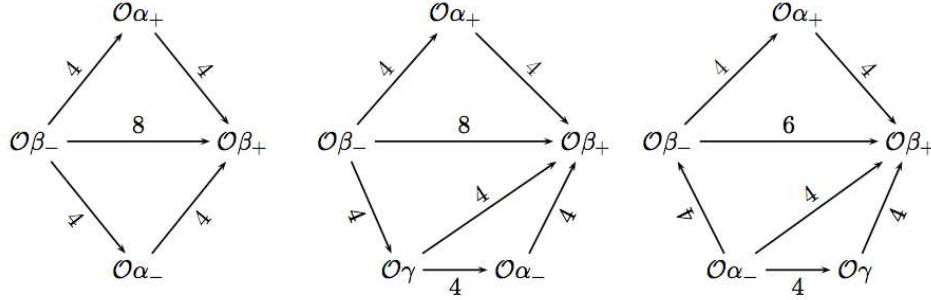

Figure 4: Heteroclinic connections in V^4. Left: $\mu_2 < \mu_2^\alpha$. Center: $\mu_2^\alpha < \mu_2 < \mu_2^\beta$. Right: $\mu_2^\beta < \mu_2$.

Proof. The existence of the invariant sphere is a consequence of a theorem by M. Field [22], which we can apply because (i) $c > 0$ is assumed small enough, and (ii) the quartic form $d_1 \|Y\|^4 + d_2 Y \cdot C^{(2)}(Y)$ is negative, where $C^{(2)}(Y)$ is the cubic map defined in Table 8 (straightforward proof if d_2 is small).

The (orbital) stability of β_+ is easy to check under the hypotheses of the theorem. We rely on [24] to assert that when $\mu_2 < \mu_2^\beta$, there is no secondary branches of equilibria than γ. Finally point (iii) follows from a careful examination of the phase portrait in the invariant subspaces, which itself relies on the sign of eigenvalues in Tables 2 and 3. ∎

In order to illustrate the phase portrait in higher dimension in the case $\mu_2 < \mu_2^\alpha$, we consider the 3 dimensional subspace $Fix(\mathbf{D}_2 \oplus \mathbb{Z}_2{}^c)$. This space contains three copies P, P' and $P"$ of $Fix(\mathbf{D}_4 \oplus \mathbb{Z}_2{}^c)$, which intersect all three on the same axis $L = Fix(\mathbb{O} \oplus \mathbb{Z}_2{}^c)$. Using coordinates (y_0, y_{2r}, y_{4r}) (see Table 1), these planes have equations $y_{2r} = 0$ and $y_{2r} = \pm(\sqrt{10}/4 y_0 - \sqrt{7/2} y_{4r})$. We note $L = \{y_{2r} = 0, y_{4r} = \sqrt{5/14} y_0\}$. The three planes are exchanged by the action of $N(\mathbf{D}_2)/\mathbf{D}_2 \simeq D_3$ (we note $N(\mathbf{D}_2)$ the normalizer of $\mathbf{D}_2$ in $\mathbf{SO}(3)$, which is known to be $\mathbb{O}$ [26]). This structure is sketched in Fig. 5.

Assuming the existence of the flow-invariant sphere, the bounded dynamics restricts to that sphere and can be projected on a 2D picture, see Fig. 6 for cases $\mu_2 < \mu_2^\alpha$ and $\mu_2 > \mu_2^\beta$. We see that β_+ and $\tilde\beta_+$ are sinks, β_- and β''_- have robust connections to α_- (in $Fix(\mathbf{D}_4 \oplus \mathbb{Z}_2{}^c)$) which itself has a robust connection to $\tilde\beta_+$. This combined with the phase portrait in $Fix(\mathbf{D}_3 \oplus \mathbb{Z}_2{}^c)$ gives a good description of the various connections in $Fix(\mathbb{Z}_2{}^c)$.

5   Bifurcations involving the modes with $\ell = 3$

Even under the hypotheses of Proposition 1, the high dimensionality of the phase space V makes it very likely that the bifurcation diagram and dynamics are so complicated that their complete
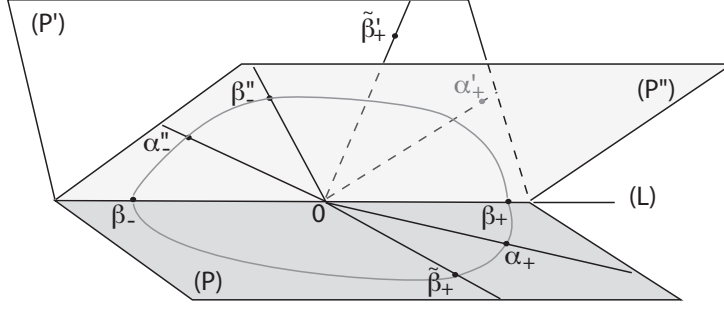
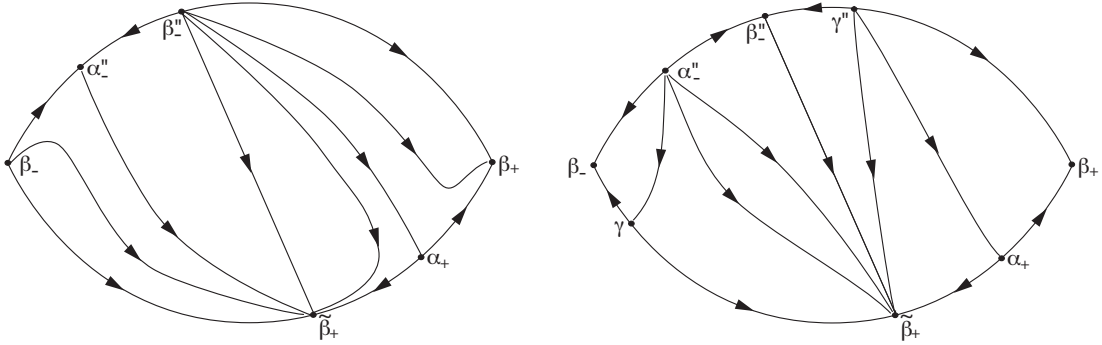Figure 5: The subspace $Fix(\mathbf{D}_2 \oplus \mathbb{Z}_2{}^c)$.

Figure 6: $Fix(\mathbf{D}_2 \oplus \mathbb{Z}_2{}^c)$: the phase portrait on the portion of invariant sphere bounded by P and P'' with $y_0 > 0$. **Left:** $\mu_2 < \mu_2^\alpha$. **Right:** $\mu_2 > \mu_2^\beta$.

description is either intractable or extremely laborious. We shall therefore restrict our analysis to subdomains in parameter space, in which spatio-temporally interesting dynamics is likely to bifurcate.

To be more precise, we now assume $\mu_1 < 0$. This implies that the modes with $\ell = 3$ are (weakly) stable at bifurcation. As we shall see, this assumption helps isolating complex spatio-temporal patterns that can be analyzed on the center manifold using the tools of equivariant bifurcation and dynamics. Actually, when $\mu_1 > 0$ various kinds of steady-state, periodic, quasiperiodic or chaotic dynamics can be observed numerically, as it can be expected from the signs of eigenvalues of the Jacobian matrix at the pure $\ell = 4$ equilibria. Our aim is at isolating regions in parameter space at which as simple as possible recurrent dynamics can be observed. Such conditions are defined in this section, and the resulting invariant objects (generalized heteroclinic cycles) will be discussed in the next section.

5.1 Dynamics in the mixed mode plane $\Pi = Fix(\mathbb{O}^-)$

We assume the hypotheses of Proposition 1 are fulfilled. Hence the $O(3)$-orbit of the octahedral steady-state β_+ is an attractor in the space V^4. We now look at the stability of β_+ in the invariant plane Π, the coordinates of which are x_{2i} and $y_{4r} = \eta y_0$ ($\eta = \sqrt{5/14}$), and which is the only invariant plane containing $\beta_\pm$ equilibria.

Π contains only the axis of symmetry $\{x_{2i} = 0\}$. Using y_0 as a parameter for this axis, the

15

equations for the flow on Π read

$$\dot{x}_{2i} = \mu_1 x_{2i} + 12 x_{2i} y_0 + (2\gamma_1 + 20\gamma_2) x_{2i}^3 \tag{15}$$

$$\dot{y}_0 = \mu_2 y_0 + 14 c y_0^2 - 14 x_{2i}^2 + (12/7 d_1 - 16/49 d_2) y_0^3 \tag{16}$$

The bifurcation scenario for this kind of planar system is classical and we don't go into details of the calculations [13]. Let us assume first that $c = 0$ and fix $\mu_2 > 0$. It follows from the above equations that a (secondary) bifurcation occurs from β_+ when μ_1 reaches the value

$$\tilde{\mu}_1 = -12 \sqrt{\frac{\mu_2}{-D}} \tag{17}$$

where $D = 12/7 d_1 - 16/49 d_2 < 0$ (see (12). This corresponds to the value of μ_1 at which the eigenvalue $\sigma_0^{\beta_+} = 0$ (see Table 3).

As μ_1 is varied the following sequence of events occurs:

- For $\mu_1 < \tilde{\mu}_1$, there exist no equilibria off the invariant axis and $\beta_\pm$ are both sinks in Π.

- At $\mu_1 = \tilde{\mu}_1$ a pitchfork bifurcation occurs from β_+ off the axis. We note δ and $\tilde{\delta}$ the bifurcated equilibria with isotropy $\mathbb{O}^-$ (which are exchanged by taking x_{2i} to $-x_{2i}$).

- As μ_1 is increased further, a Hopf bifurcation occurs from δ (and $\tilde{\delta}$). We call C_Π and $\tilde{C}_\Pi$ the bifurcated periodic orbits.

- The two limit cycles grow until they collide with the stable manifold of the origin. Then they disappear and two *saddle-sink connections* from β_+ to β_- are established in Π at a value $\mu_1 = \hat{\mu}_1$ which satisfies $\tilde{\mu}_1 < \hat{\mu}_1 < 0$, see Fig. 7.

- The equilibria δ, $\tilde{\delta}$ die off at the origin in a "reverse" bifurcation at $\mu_1 = 0$.

- The heteroclinic orbit from β_+ to β_- persists until a new pitchfork bifurcation occurs from β_- at a positive value of μ_1.

These properties persist when $c \neq 0$ is small enough.
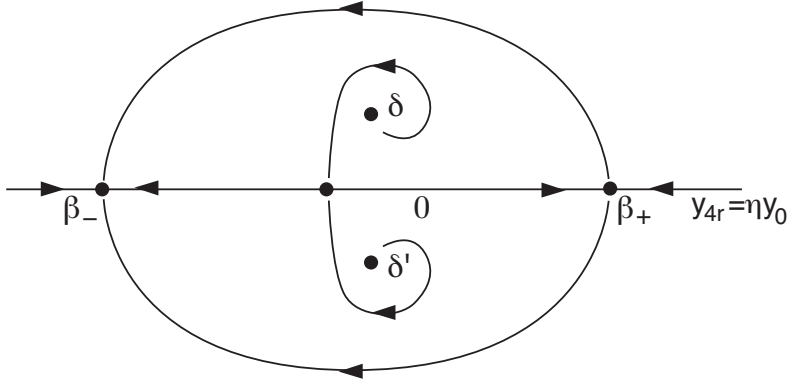
Figure 7: Sketch of the phase portrait in Π when $\hat{\mu}_1 < \mu_1 < 0$.

5.2 Dynamics of mixed modes off the plane Π

We now want to find conditions on parameters such that the heteroclinic connections found above, not only exist but also drive the dynamics along the $\ell = 3$ modes. Then the construction of the generalized heteroclinic cycles will follow.

Let us denote by $y_0^{\alpha_\pm}$ (resp. $y_0^{\beta_\pm}$) the value of y_0 on the branches of equilibria $\alpha_\pm$ (resp. $\beta_\pm$) at a given parameter value $\mu_2 > 0$.

Definition 2 *We set $\mu'_1 = -7y_0^{\alpha_+}$ (value at which $\sigma_2^{\alpha_+} = 0$) and $\mu''_1 = -2y_0^{\beta_+}$ (value at which $\sigma_2^{\beta_+} = 0$).*

Note that $\mu'_1 < 0$ and $\mu''_1 < 0$. The following lemma gives conditions on the parameters such that the eigenvalues of the Jacobian matrix of $\alpha_\pm$, $\beta_\pm$ along the modes $\ell = 3$ are mostly negative.

Lemma 2 *We suppose $\mu_1 < 0$. Then:*
(i) $\sigma_j^{\alpha_+} < 0$ ($j = 0, 1, 3$), $\sigma_2^{\alpha_-} < 0$, $\sigma_1^{\beta_+} < 0$, $\sigma_0^{\beta_-} < 0$ and $\sigma_2^{\beta_-} < 0$.
(ii) if $\mu_1 < \min(\mu'_1, \mu''_1)$, then $\sigma_j^{\alpha_-} < 0$ ($j = 0, 1, 3$), $\sigma_2^{\alpha_+} < 0$, $\sigma_1^{\beta_-} < 0$ and $\sigma_2^{\beta_+} < 0$;
(iii) If $\mu_1 < \min(\mu'_1, 6\mu''_1)$, then in addition to inequalities (ii), we also have $\sigma_0^{\beta_+} < 0$.

Proof. Point (i) follows straightforwardly from Tables 2 and 3. It also follows from these tables that the signs of the eigenvalues in point (ii) are true if

$$\mu_1 < 6y_0^{\alpha_-} \quad , \mu_1 < -7y_0^{\alpha_+}, \quad \mu_1 < 6y_0^{\beta_-}, \quad \mu_1 < -2y_0^{\beta_+}.$$

Solving (12) and (11) for y_0, we find that

$$
\begin{aligned}
y_0^{\alpha_\pm} &= \frac{1}{2(d_1 + d_2)} \left(-9c \mp \sqrt{81c^2 - 4(d_1 + d_2)\mu_2} \right) \\
y_0^{\beta_\pm} &= \frac{1}{D} \left(-7c \mp \sqrt{49c^2 - D\mu_2} \right)
\end{aligned}
$$

Recall that $d_1 + d_2 < 0$ and $D < 0$ (see 12). Replacing these formulas in the above inequalities, point (ii) follows. Also note that $6\mu''_1 = \tilde{\mu}_1$, from which (iii) follows. ∎

By point (iii) of this lemma, if $\mu_1 < \min(\mu'_1, 6\mu''_1)$, all the eigenvalues of the Jacobian matrix at β_+ in eigendirections transverse to the **O**(3)-orbit are negative, therefore β_+ is an orbitally stable equilibrium (i.e. its orbit $\mathcal{O}_{\beta_+}$ is an asymptotically stable object). However for the values of the coefficients d_1 and d_2 shown in Fig. 2.3, and with c close to 0, one can check the inequalities

$$6\mu''_1 < \mu'_1 < \mu''_1$$

Moreover, although it is cumbersome to determine the value $\hat{\mu}_1$ at which the saddle-sink connection $\beta_+ \to \beta_-$ is established in Π, numerical simulations in 7.1 show evidence that $\hat{\mu}_1 < \mu''_1$. To understand the change of dynamics when μ_1 varies in the interval $(6\mu''_1, \mu''_1)$ it is convenient to consider the 3-dimensional invariant space $\Delta = Fix(\mathbf{D}_4^d)$. Note that $\Delta = P \oplus \Pi$ (see Table 1). The eigenvalues $\sigma_2^{\alpha_+}$, resp. $\sigma_2^{\beta_+}$, correspond to the eigendirection at α_+, resp. at $\tilde{\beta}_+$, orthogonal to P in Π, see Fig. 8. When μ_1 increases to cross μ'_1, $\sigma_2^{\alpha_+}$ changes sign from < 0 to > 0, which corresponds to the *reverse* pitchfork bifurcation of a mixed-mode equilibrium in Π. It can be shown (see [18] for a similar case) that in this case a saddle-sink connection is established in Π between α_+ and $\tilde{\beta}_+$.
The dynamics in Π when $\mu_2 < \mu_2^\alpha$ and $\max(\hat{\mu}_1, \mu'_1) < \mu_1 < \mu''_1$ is sketched in Fig. 8.

In fact, as in the Proposition 4.6 of [18], one can even show the following result in the 5-dimensional subspace $Z = Fix(\mathbb{Z}_4^-)$. We refer to [18] for the proof.

Proposition 2 *If $c > 0$, $\mu_2 > 0$ and $\hat{\mu}_1 < \mu''_1$, there exists an open interval of negative values of μ_1 such that the full (4-dimensional) unstable manifold of α_+ is included in the stable manifold of the group orbit of β_+ in Z.*
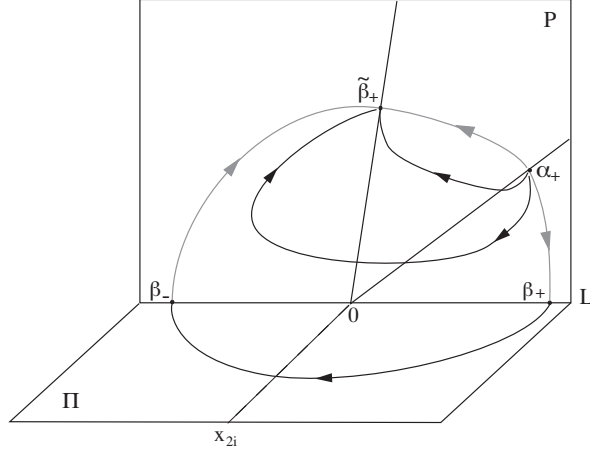
Figure 8: The phase portrait in $\Delta = Fix(\mathbf{D}_4^d)$ (in grey the heteroclinic connections in P).

6 Existence of heteroclinic cycles

6.1 Generalized heteroclinic cycles

We summarize the results of sections 4 and 5 in the following theorem:

Theorem 1 *For the system (9) with coefficient values as in Fig. 2.3, assume $c > 0$ close to 0 and $\max(\hat{\mu}_1, \mu_1') < \mu_1 < \mu_1''$. Then*

(i) *If $0 < \mu_2 < \mu_2^\alpha$, the following sequence of robust heteroclinic connections (saddle-sink connections in flow-invariant subspaces) exists:*
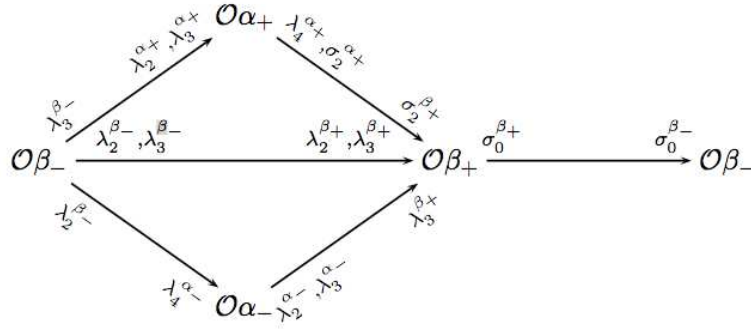
(ii) *If $\mu_2^\alpha < \mu_2 < \mu_2^\beta$, a similar object as in (i) exists, with an additional orbit of equilibria γ intercalated between $\mathcal{O}\beta_-$ and $\mathcal{O}\alpha_-$, see Fig. 4 (center).*

(iii) If μ_2 is slightly larger than μ_2^β, the sequence of connections is simpler (α_- not involved in the sequence):
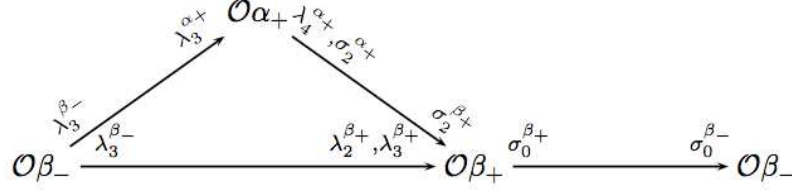
We indicate in the diagrams the eigenvalues for the corresponding stable or unstable parts of the heteroclinic connections. Note that the unstable manifold of each equilibrium is filled with heteroclinic orbits connecting to one or several other equilibria..

The above sequences realize generalized heteroclinic cycles *of types I(i), I(ii) and I(iii) respectively.*

Proof. By inspection of the diagrams in Fig. 4 and Proposition 2. ∎

6.2 A simple heteroclinic cycle involving mixed-mode equilibria

We have seen in Section 5.1 that when $\mu_1 < \hat{\mu}_1 < 0$, the presence of a stable fixed point δ in the plane Π prevented the existence of the saddle-sink connections in that plane. However if we now look at the 3-dimensional subspace $\Delta = P \oplus \Pi$, a saddle-sink connection can exist in that subspace between δ (in Π) and $\tilde{\beta}_+$ (in P). A similar situation holds in the $\ell = 1, 2$ interaction [13]. Here the process by which this saddle-sink connection is established is more complex than in the $\ell = 1, 2$ case. It results from a sequence of bifurcations of steady-states and/or periodic orbits off the invariant planes and is numerically analyzed in Section 7.2.

Once the saddle-sink heteroclinic connection exists, a heteroclinic cycle is set since $\tilde{\beta}_+$ belongs to the group orbit $\mathcal{O}\beta_+$ (see the diagram 18 below).

$$(18)$$

Moreover this cycle is *simple*, in the sense that it involves unstable of dimension 1 only. Following [13] we call it a type II heteroclinic cycle.

Remark that the full cycle is included in the 5 dimensional subspace $Z = Fix(\mathbb{Z}_4^-)$. Indeed, δ is connected in P to β_+ and $\tilde{\beta}_+$. But $\tilde{\beta}_+$ is connected to $\tilde{\delta}$ inside the image $\tilde{\Pi}$ of Π by the 8 fold rotation with vertical axis, which is itself included in $\tilde{\Delta} = \{x_{2r}, y_0, y_{4r}\}$. Now note that $Z = \Delta + \tilde{\Delta}$.

Variants of this cycle, involving periodic orbits in Π, can also exist for suitable parameter values.

7 The numerical simulation of the dynamics on the center manifold and its interpretation

The results of the previous section do not guarantee the observability of intermittent dynamics induced by the presence of heteroclinic cycles, if they exist. This depends on the behavior as time increases, of trajectories starting close to the cycle. Obviously if the (generalized) heteroclinic cycle is an attractor, then the nearby dynamics will show aperiodic switching between steady-states with increasing periods of time passed in their vicinity. Even if a heteroclinic cycle is not asymptotically stable, a nearby attractor can exist, so that the intermittent behavior can be observable.

19

Stability conditions have been derived in [27] for heteroclinic cycles which are called "simple". These conditions are easily applicable to cycles of type II, Section 6.2. As a general rule, stability depends upon the relative strength of contracting v.s. expanding eigenvalues at the steady-states in the heteroclinic cycle. The case of generalized heteroclinic cycles, like those of type I (section 6.2) is more difficult to analyze. Already in spherical Rayleigh-Bénard convection with $\ell = 1$ and 2 mode interaction, the characterization of the asymptotic stability of generalized heteroclinic cycles led to non obvious formulas [18]. In the present situation the analysis is even more complicated due to the complex topology of these cycles.

In this section we therefore explore the dynamics on the center manifold by time integrating the equations (9). We first determine the "stability curves" which, in the (μ_1, μ_2) plane, correspond to the critical values which have been defined in Sections 4 and 5. Then the bifurcation diagrams when μ_1 is varied are computed, and the dynamics is explored for selected values of μ_1, μ_2 and c. Results are compared with eigenvalues computed for the same parameter values, which correspond to the rates of contraction and expansion at relevant steady-states.

7.1 Stability diagrams

We focus on the parameter domain delimited by $\mu_1 < 0$ and $\mu_2 > 0$. This domain is subdivided into regions bounded by "neutral stability curves" on which the eigenvalues of the $\alpha_\pm$ and $\beta_\pm$ equilibria change sign (Figs. 9 and 10). The names of the corresponding 'critical' values of μ_1 have been defined in prevoius sections. See Tables 2 and 3 for an expression of the leading part of these eigenvalues. The eigenvalue becomes positive when the associated stability curve is

Figure 9: Stability diagrams of equilibria $\alpha_\pm$ and $\beta_\pm$ for $g(r) = 1/r^2$ and two values of the coefficient c: (left) $c = 0.04$ and (right) $c = 0.004$. For μ_2 fixed, μ_{eq}^σ denotes the μ_1 value at which the eigenvalue value σ of the equilibrium eq. changes sign. See Tables 2 and 3 for the other critical values notations.

crossed by increasing μ_1. These domains differ only slightly between both force fields in $1/r^2$ and $1/r^5$. In contrast, the bifurcation parameter c has a strong influence on the region size for each force field. However in any case, the following inequalities hold when $\mu_2 > 0$ is small
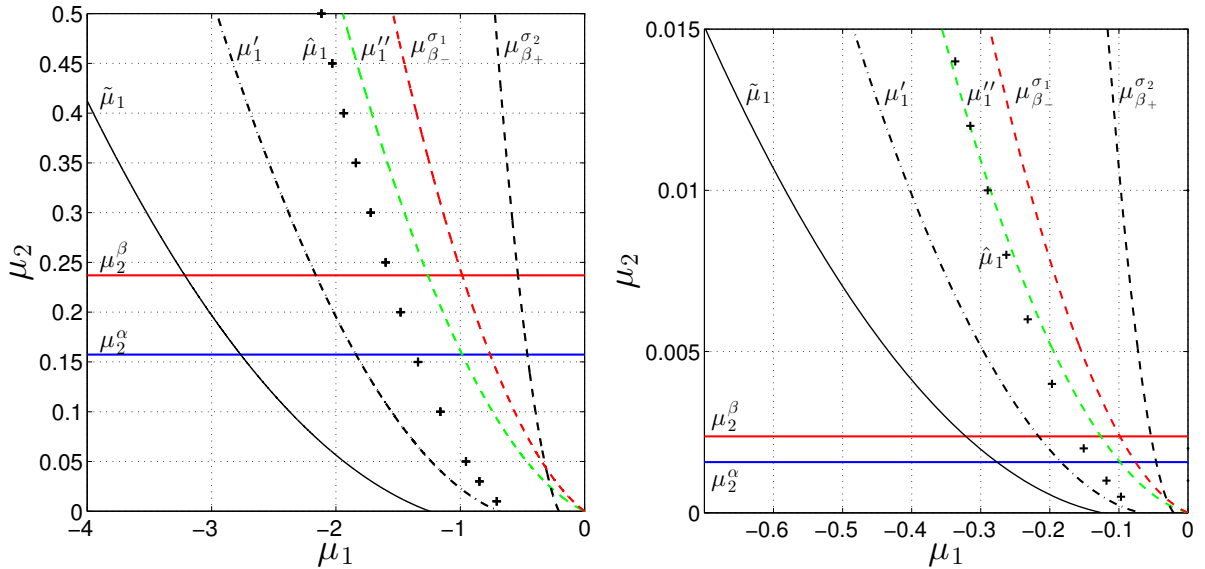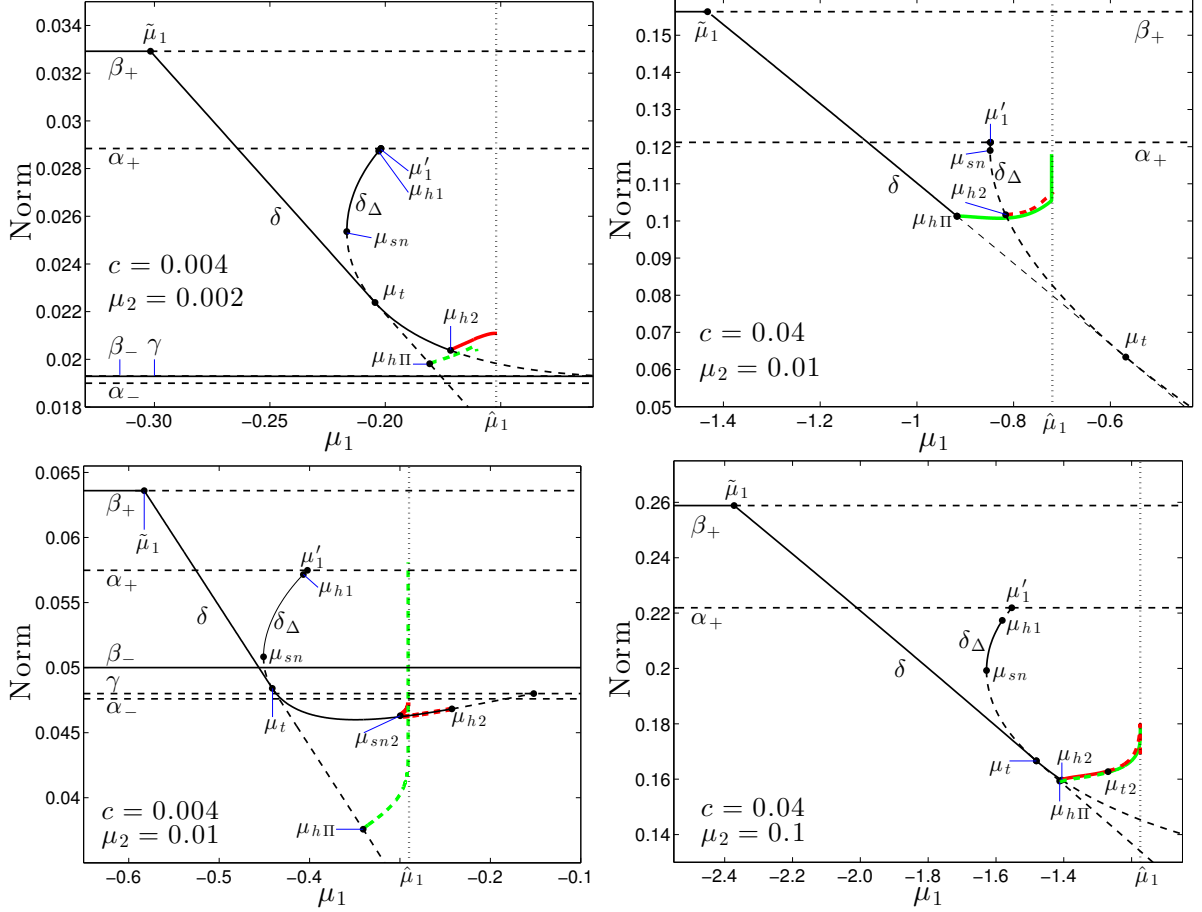
Figure 10: Stability diagrams of equilibria $\alpha_\pm$ and $\beta_\pm$ for $g(r) = 1/r^5$ and two values of the coefficient c: (left) $c = 0.04$ and (right) $c = 0.004$. Notations are as in Fig. 9

enough:

$$\tilde{\mu}_1 < \mu_1' < \hat{\mu}_1 < min(\mu_1'', \mu_{\beta_-}^{\sigma_1}, \mu_{\beta_+}^{\sigma_2}) \tag{19}$$

where μ_{eq}^σ denotes the value of μ_1 at which the eigenvalue σ of the equilibrium eq. changes sign (hence becomes positive when $\mu_1 > \mu_{eq}^\sigma$). In consequence, according to Theorem 1, when μ_2 is small enough and $\hat{\mu}_1 < \mu_1 < min(\mu_1'', \mu_{\beta_-}^{\sigma_1}, \mu_{\beta_+}^{\sigma_2})$, heteroclinic cycles exist.

Note that for $c = 0.004$ and when μ_2 is large enough, $\hat{\mu}_1$ becomes larger than μ_1'' (Figs. 9b and 10b). In this case the heteroclinic cycles are necessarily unstable along transverse directions. Numerical simulations show a seemingly unstructured dynamics with no intermittent behavior, we therefore do not consider this case.

To study the bifurcation scenarios which lead to the establishment of heteroclinic cycles, we keep μ_2 fixed while μ_1 is increased from $\tilde{\mu}_1$ up to the value at which intermittent behavior is lost. A priori we have to distinguish three cases depending on the relative position of μ_2 with respect to μ_2^α and μ_2^β. However it is observed that the numerical results display similar dynamics in the different cases.

We focus on the central force field $g(r) = 1/r^2$. The case $g(r) = 1/r^5$ shows very similar results.

7.2 Steady-state and Hopf bifurcations in $\Delta = Fix(D_4^d)$

We noticed in Section 6 that a key condition for the existence of heteroclinic cycles is the establishment of saddle-sink heteroclinic connections between steady-states in the three-dimensional space $\Delta = P \oplus \Pi$. Figure 8 shows the phase portrait in the flow-invariant domain $y_{4r} < \eta y_0$, in the dynamically simple case $\mu_1 \in]max(\hat{\mu}_1, \mu_1'), \mu_1''[$. Here we study in more details, with the help of the continuation software AUTO [1], the bifurcation diagrams and the scenarios which lead to these connections in Δ for $c = 0.004$ and $c = 0.04$.

The results are displayed in Fig. 11 for $\mu_2 = 0.002$ and 0.01 (case $c = 0.004$), and $\mu_2 = 0.01$ and 0.1 (case $c = 0.04$). These values illustrate the cases described in Theorem 1. The presence of a "submaximal" equilibrium γ in P does not introduce significant differences in the bifurcation

Figure 11: Bifurcation diagrams in Δ with respect to μ_1 for four different parameter couples (μ_2, c). [Dashed] Plain line indicates [unstable] stable branch. The dotted vertical line corresponds to the value $\hat{\mu}_1$.

diagrams.

We indicate in each case the value $\hat{\mu}_1$ at which the saddle-sink connection $\beta_+ \to \beta_-$ is established in Π. This happens when the stable manifold of the periodic orbit which bifurcates from δ in Π at $\mu_1 = \mu_{1\Pi}$, meets the stable manifold of the origin (Section 5.1).

Horizontal lines correspond to equilibria $\alpha_\pm$, $\beta_\pm$ and γ in P, which do not depend on μ_1. The α_- and β_- equilibria do not appear in right diagrams (Fig. 11) in order to focus on the relevant bifurcations. The straight line with negative slope corresponds to the branch δ equilibrium in Π, which bifurcates from β_+ at $\tilde{\mu}_1$. It ends up at the origin for values of μ_1 which are not shown here. The following list shows the typical sequence of bifurcations for equilibria and periodic orbits emerging off the invariant planes in Δ.

- At $\mu_1 = \mu_1'$ an equilibrium δ_Δ bifurcates from α_+ (pitchfork bifurcation). The bifurcated branch is subcritical and unstable.

- At $\mu_1 = \mu_{h1}$ a Hopf bifurcation occurs along this branch, after which δ_Δ becomes stable. Note that μ_{h1} is very close to μ_1' in all cases.

- At $\mu_1 = \mu_{sn}$ the branch δ_Δ bends back and looses stability (saddle-node bifurcation).

- This unstable branch crosses the branch of δ equilibria in the plane Π at $\mu_1 = \mu_t$ and becomes stable again (transcritical bifurcation).

- At $\mu_1 = \mu_{h2}$, another Hopf bifurcation occurs on the δ_Δ branch. We call C_2 these periodic orbits.

- Finally the equilibria δ_Δ merge with the β_- or γ branch (depending on whether $\mu_2 \leq \mu_2^\beta$ or $\mu_2 > \mu_2^\beta$), via a reverse pitchfork bifurcation.

Note that μ_{h2} and $\mu_{h\Pi}$ have the same position relative to μ_t.

7.3 Numerical time integration in V

We take on the bifurcation scenarios in Δ, Fig. 11, to describe the dynamics that arise in V as μ_1 is varied in the corresponding range of values.

7.3.1 The case $c = 0.004$.

We fix $\mu_2 = 0.01$, a value larger than μ_2^β. Similar behavior was found when $\mu_2 = 0.002 \in]\mu_2^\alpha, \mu_2^\beta[$ or when $\mu_2 = 0.001 < \mu_2^\alpha$, although in these cases an additional equilibrium γ exists in P. In fact, in these ranges of parameter values, most of the dynamics in V is driven by the dynamics in Δ or Z.

The simulations are performed by increasing μ_1. By stability of an equilibrium in V we mean that its $O(3)$ orbit is an attractor (orbital stability).

- For $\mu_1 < \tilde{\mu}_1$, time integration confirms that β_+ (i.e. its $O(3)$ orbit) is the unique sink in V.

- As μ_1 crosses $\tilde{\mu}_1$, bifurcated equilibria δ in Π become the unique sinks untill μ_1 reaches $\mu_{sn} = -0.45094$, value at which the equilibria of type δ_Δ become stable too via the saddle node bifurcation in Δ. This bistability persists until μ_1 crosses μ_t. Then δ_Δ are the only stable equilibria.

- At $\mu_{h1} = -0.40690$, δ_Δ becomes unstable through Hopf bifurcation followed by a period doubling cascade in a narrow range inside the interval $]\mu_{h1}, \mu_1'[$ ($\mu_1' = -0.40239$). Then a strange attractor appears in in the vicinity of α_+ in D, called the 'mussel' because of its shape (Fig. 12).

- The periodic orbit disappears at $\mu_{hom} \simeq -0.40605 < \mu_1'$ through a homoclinic bifurcation with α_+. Then a heteroclinic connection from δ_Δ to α_+ is established (Fig. 13). Moreover the connection δ to δ_Δ is established at $\mu_1 = \mu_t < \mu_{hom}$. Thus in the narrow range $]\mu_{hom}, \mu_1'[$ the following sequence of heteroclinic orbits exists in Δ: $\beta_+ \rightarrow \delta \rightarrow \delta_\Delta \rightarrow \alpha_+ \rightarrow \beta_+$ or $\tilde{\beta}_+$. But from $\tilde{\beta}_+$ a similar sequence of connections in the space $\tilde{\Delta} = \{x_{2r}, y_0, y_{4r}\}$, which is the image of Δ is the 8-fold rotation around vertical axis. This heteroclinic cycle belongs to Z for the reason given in Section 6.2. In fact this is a (non simple) variant of the heteroclinic cycle of type II described there.
  This object is unstable. Instead, it is observed that two strange attractors alternate in an irregular manner (see the time series in Fig. 14). The first one is close to the 'mussel' attractor. The second one, of larger amplitude, first skirts the connections between α_+ and a β_+ type steady-state, then approaches the 'mussel' attractor with a spiraling trajectory (see phase portrait in Fig. 14). The intermittent behavior (aperiodic alternation of the dynamics along the two 'cones' in the 'twin-cone' attractor) is a consequence of
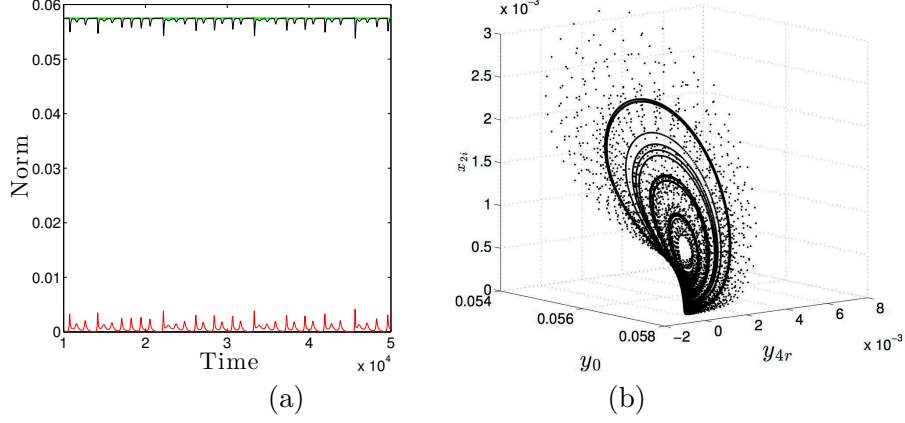
23

Figure 12: The 'mussel' attractor at $\mu_1 = -0.4061$, $\mu_2 = 0.01$, $c = 0.004$. (a) Time series of 'energies' (norms) of the $\ell = 3$ modes (red) and 4 modes (black). Green line: norm of α_+. (b) Phase portrait in Δ.
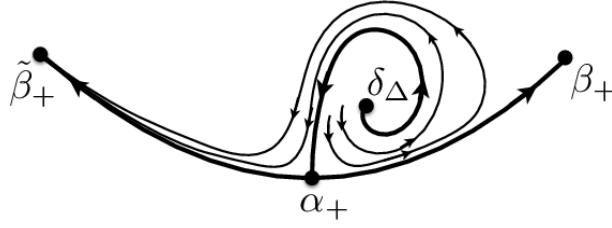

Figure 13: Sketch of the phase portrait in Δ near α_+ when μ_1 slightly lower than μ_1'.

the duplication of the same dynamics in Δ and $\tilde{\Delta}$. The dynamics spends long times near the axisymmetric state α_+. The right panel in Fig. 14 shows that the dynamics near the mussel attractor is nearly contained in Δ or in $\tilde{\Delta}$: the component x_{2i} is almost zero when $y_{4r} < 0$. This dynamics is stable and it is an attractor in the whole space V.

- As μ_1 is further increased, the 'mussel' attractor becomes barely observed in the dynamics.

- After μ_1 has crossed μ_1', α_+ becomes unstable in the x_{2i} direction in Δ, hence the above heteroclinic cycles disappears and only seemingly periodic dynamics are observed, depending on initial conditions: one follows the 'mussel', the other one the 'twin-cone', Fig. 15.

- The number of loops of the twin-cone decreases (three at $\mu_1 = -0.37$, two at $\mu_1 = -0.36$) as μ_1 increases further, till the attractor disappears at $\mu_1 \sim -0.35$. In contrast the amplitude of the other attractor increases till the attractor boundary comes near the invariant planes Π and its copy $\tilde{\Pi}$ in $\tilde{\Delta}$ (Fig. 16, left panel). Indeed the dynamics passes near the limit cycle C_Π (bifurcated from δ at $\mu_{h\Pi} = -0.3407$) or near its copy in $\tilde{D}$.

- At $\mu_1 = -0.2967$ the attractor becomes asymmetric as shown in Fig. 16 right panel. Unspecified perturbation of this attractor leads to a slightly modified attractor in V. The amplitude is smaller and the period shorter. Note that in this range of values of μ_1, the limit cycles C_2 bifurcated from δ_Δ at $\mu_{h2} = -0.2997$ exists but is unstable in V.
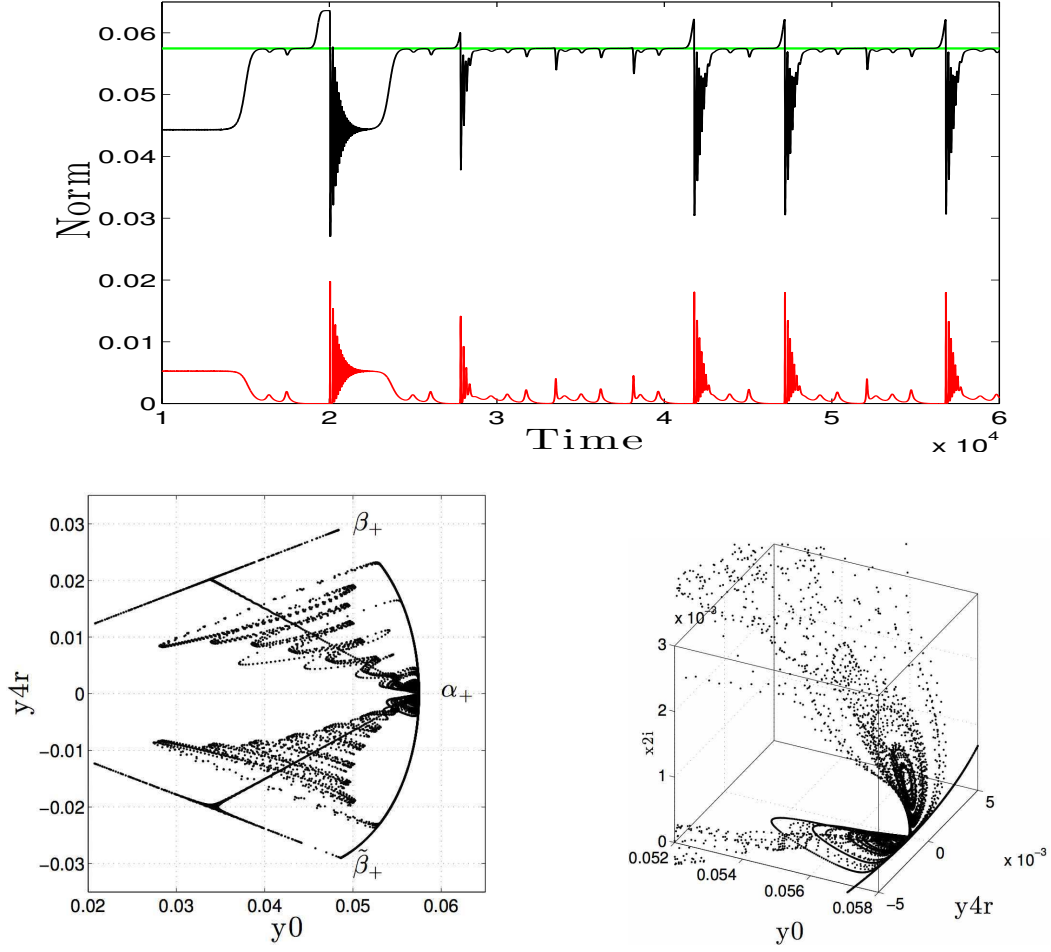
24

Figure 14: Dynamics in Z at $\mu_1 = -0.40605$, $\mu_2 = 0.01$, $c = 0.004$. Above: time series (same color code as in Fig. 12). Below left: projection of the phase portrait on P. The initial condition is close to the type II heteroclinic cycle. Skew line in the left panel correspond to the C_Π periodic branch or its copy in $\tilde{\Pi}$. After one cycle the dynamics converges to the 'twin-cone' strange attractor. Below right: magnification near α_+ showing the 'mussel' attractor in Δ.

- Close to the emergence of the heteroclinic connection β_+ to β_- ($\hat{\mu}_1 = -0.29$), the previous strange attractor loses its stability and the dynamics restricted to Z tends to β_- or its copy $\tilde{\beta}_-$. In contrast in V the dynamics is time-dependent. This dynamics is similar to the previous one during 100 to 1000 periods but interspersions by chaotic events with large bursts arise (Fig. 17).

- When $\mu_1 > \hat{\mu}_1$ the generalized heteroclinic cycle is established. However when $\mu_2 = 0.01$ we do not observe intermittent behavior related to the cycle, rather periodic or aperiodic fluctuations around either the octahedral pattern β_+ or the mixed mode, "tetrahedral-like" pattern δ. Nevertheless the simulation for $\mu_2 = 0.002$ and μ_1 close to $\hat{\mu}_1$ shows a dynamics which roughly follows parts of the generalized heteroclinic cycle, see (Fig. 18). In Annex D the eigenvalues giving the rates of expansion and contraction along the heteroclinic connections are displayed in this case. It shows that the overall contraction rate (product of the absolute value of negative eigenvalues) is larger than the expansion one, which one would expect to give asymptotic stability. However the numerical simulations indicate
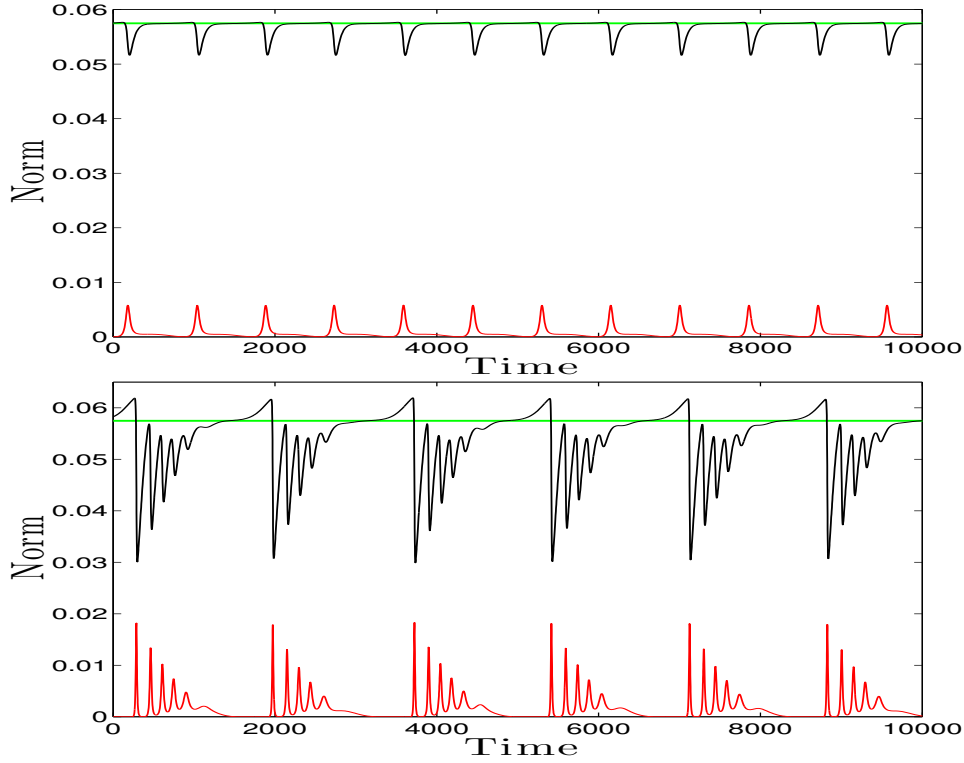
25

Figure 15: Time series of the dynamics following the 'mussel' (up) and the 'twin-cone' (down) close to α_+ for $\mu_1 = -0.4 > \mu_1'$ and $\mu_2 = 0.01$, $c = 0.004$ (same color code as in Fig. 12).

this is not the case.

- As μ_1 gets larger than $min(\mu_1'', \mu_{\beta_-}^{\sigma_1}, \mu_{\beta_+}^{\sigma_2})$, additional instabilities lead to more complex and diffuse dynamics: small amplitude dynamics are interspersed by bursts whose occurrence and amplitude increase with μ_1 (see Fig. 19).

In summary: the predicted heteroclinic cycles are unstable. Intermittent-like dynamics related to the presence of heteroclinic cycles are observed in narrow ranges of μ_1 (trajectories come near the axisymmetric state α_+ in this case). When μ_2 is small enough and $\mu_1 > \hat{\mu}_1$ (close to $\hat{\mu}_1$) the trajectories explore the vicinity of the octahedral patterns β_+ and β_- in an irregular manner but don't show a clear intermittent behavior.
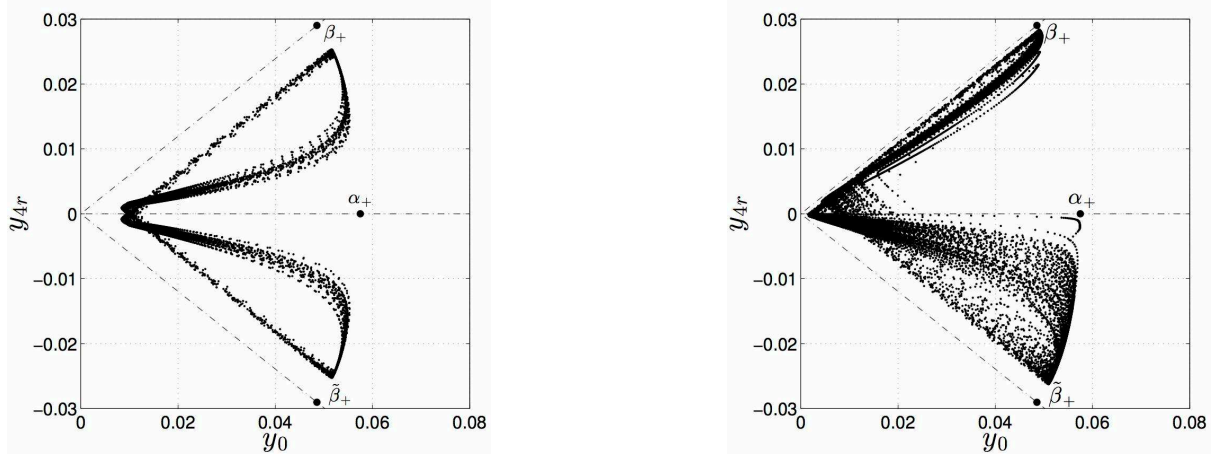
Figure 16: Projection on P of the phase portrait of the nearly periodic strange attractor for (left) $\mu_1 = -0.31$ and (right) $\mu_1 = -0.295$. Other parameters: $\mu_2 = 0.01$, $c = 0.004$. Dot dashed lines indicate the intersections with planes Π and $\tilde{\Pi}$.
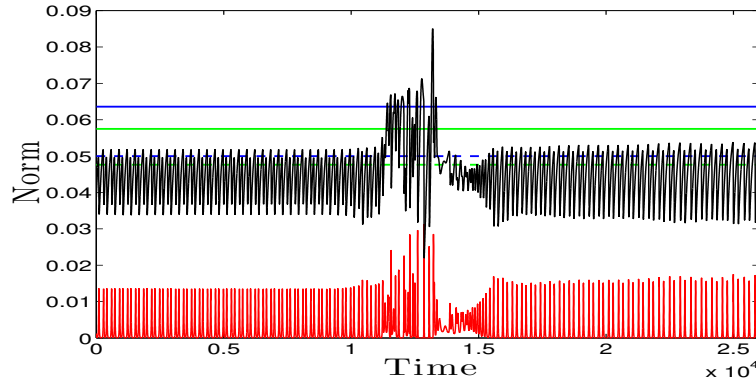
Figure 17: Interspersed 2-periodic dynamics when $\mu_1 = -0.28, \mu_2 = 0.01$, $c = 0.004$. Same color code as in Fig. 12. Green line: norm of α_+, blue line: norm of β_+, green dotted line: norm of α_-, blue dotted line: norm of β_-.

Figure 18: Time series for $\mu_1 = -0.12, \mu_2 = 0.002$, $c = 0.004$ (same color code as in Fig. 17). The plateaux near the energy of β_- correspond to a part of the periodic cycle C_2 which passes near the equilibrium γ.

27
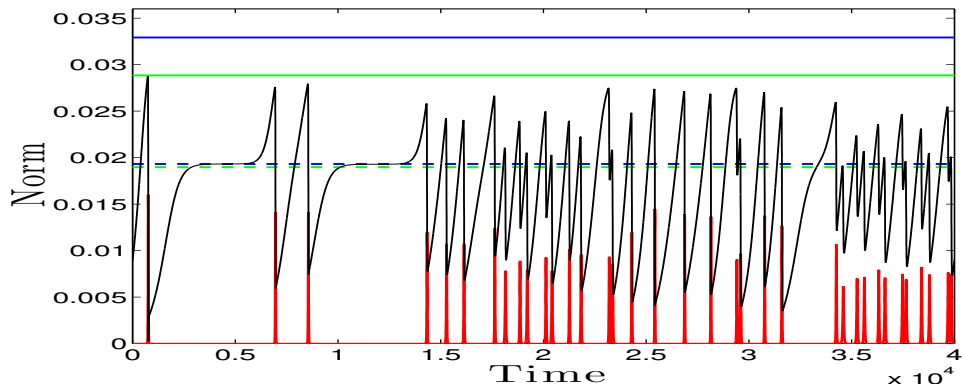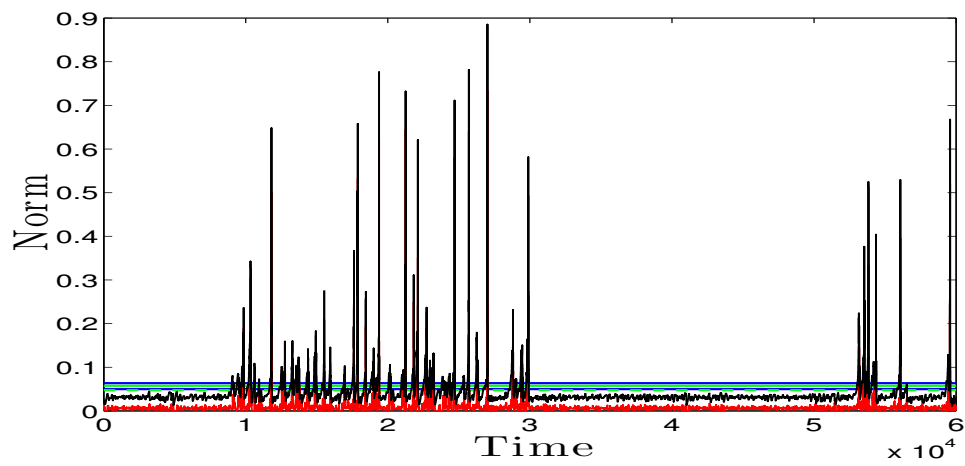
Figure 19: Time series for $\mu_1 = -0.15, \mu_2 = 0.01, c = 0.004$ (same color code as in Fig. 17).

7.3.2 The case $c = 0.04$

The values of μ_2 that we chose for the simulations ($\mu_2 = 0.01$ and 0.1) are smaller that μ_2^α, in order to keep the study within the range of validity of the center manifold approximation, see Fig. 9. Then we observe that the phase portrait in the pure mode subspace V^4 corresponds to Fig. 6 (left): the ($O(3)$-orbit of) β_+ is the unique attractor in V^4.

Even though the bifurcation diagram close to α_+ presents similarity with the case $c = 0.004$, the time integration does not show the same attractors. The dynamics converges to either the equilibrium δ or the periodic orbit C_Π in Π plane when $\mu_1 < \hat{\mu}_1$. We now list our observations as μ_1 is increased.

- When μ_1 crosses $\hat{\mu}_1$, generalized heteroclinic cycles are established. The simulation displays a dynamics which is compatible with cycle I(i) of Theorem 1: trajectories visit the vicinity of equilibria β_+ and β_- although β_- may be missed during several cycles, figures 20 and 21. The axisymmetric steady-state α_- is also visited occasionally. The fact that equilibria of type β_- are "missed" on a recurrent basis indicates that the heteroclinic cycle itself is not asymptotically stable, but rather that an attractor exists in a neighborhood of it. We suggest the following interpretation: when μ_1 is close to $\hat{\mu}_1$ the connection $\beta_+ \to \beta_-$ in Π is strongly attracted toward the axis $L = Fix(\mathbb{O} \oplus \mathbb{Z}_2^c)$ before it joins β_-. Indeed this is close to the 'homoclinization' of the periodic orbit C_Π on the origin and β_+. Nearby trajectories may then follow the stable manifold of β_- in Π, but from the neighborhood of 0 it may instead follow an orbit along the stable manifold of $\tilde{\beta}_+$ or α_-, which are both sinks in P. When the trajectory joins directly β_+, this dynamics follows the periodic cycle C_2 which exist (but is unstable) for a slightly larger value than $\hat{\mu}_1$ as we saw in Section 7.2.

- After μ_1 is slightly increased this cycle vanishes through a heteroclinization on the equilibria β_+, 0 and α_+. Then the time series show the presence of two plateaux at equilibria of types β_- and β_+, at each cycle (Figs. 22 and 23). Note that for $\mu_2 = 0.01$, the plateau near β_+ is not really visible (Fig. 23), it means that the trajectory does not spend long time close to the β_+ equilibria. It is a consequence of the fact that $|\mu_2| \ll |\mu_1|$ so that β_+ has small contracting eigenvalues (order of μ_2) compared of its unstable direction (order of $|\mu_1|$). When μ_2 is larger, equal to 0.1, in contrast both plateaux have a similar duration (Fig. 22).

- Even though the generalized heteroclinic cycle may not be stable, the simulations show that a nearby attractor exists. However, by increasing further μ_1, the heteroclinic cycle is gradually more unstable: one or both equilibria are not reached anymore. Thus, for a value of μ_1 which is still smaller than $min(\mu_1'', \mu_{\beta_-}^{\sigma_1}, \mu_{\beta_+}^{\sigma_2})$ the dynamics is no more a heteroclinic cycle. Nevertheless, this attractor gets the main characteristic of the β-heteroclinic cycle: the trajectory spends a long time in V^4 following by a short transition in the mixed mode space D (Fig. 24).

- For larger values of μ_1 we observe isolated burst of large amplitudes as in the case $c = 0.004$ (Fig. 25). The frequency of burst occurrence and their amplitude increases when μ_1 approaching zero. Moreover the component of mode 3 does not vanish anymore.

In summary: type I generalized heteroclinic cycles involving octahedral and axisymmetric equilibria exist in the parameter range predicted in Section 6. Numerical simulations show that the dynamics closely follow these invariant sets when μ_1 is larger than but close enough to $\hat{\mu}_1$.

However, as we already noticed in the case $c = 0.004$, it does not converge to it. This indicates that the generalized heteroclinic cycles are not attractors, although the rates of contraction and expansion of the eigenvalues along the heteroclinic connections would suggest they are, see Annex D.

Figure 20: Time series for $\mu_1 = -1.17, \mu_2 = 0.1, c = 0.04$. Same color code as in Fig. 17.

Figure 21: Time series for $\mu_1 = -0.712, \mu_2 = 0.01, c = 0.04$. Same color code as in Fig. 17.

Figure 22: Time series for $\mu_1 = -1, \mu_2 = 0.1, c = 0.04$. Same color code as in Fig. 17.
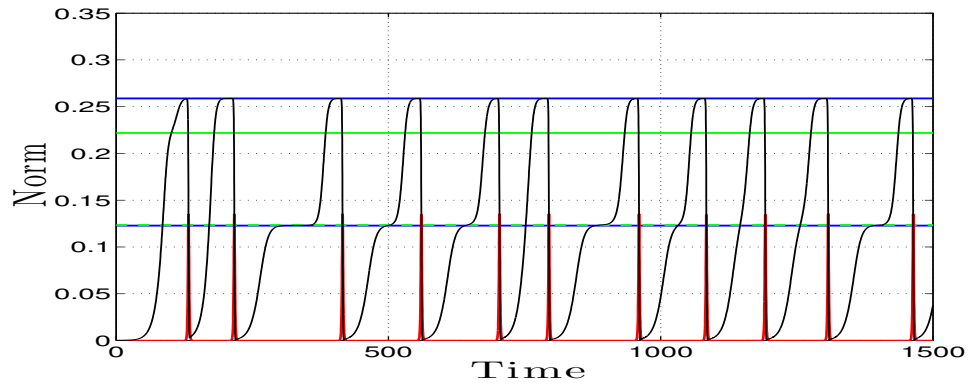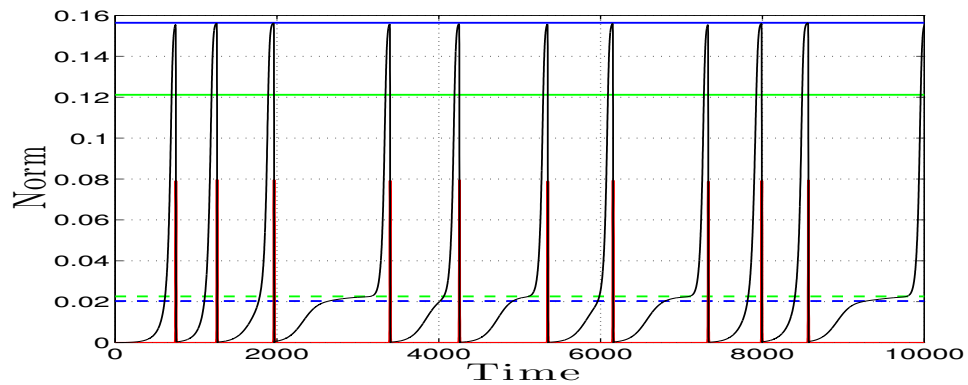
30

Figure 23: Time series for $\mu_1 = -0.61, \mu_2 = 0.01$, $c = 0.04$. Same color code as in Fig. 17.

Figure 24: Time series for $\mu_1 = -0.8, \mu_2 = 0.1$, $c = 0.04$. Same color code as in Fig. 17.

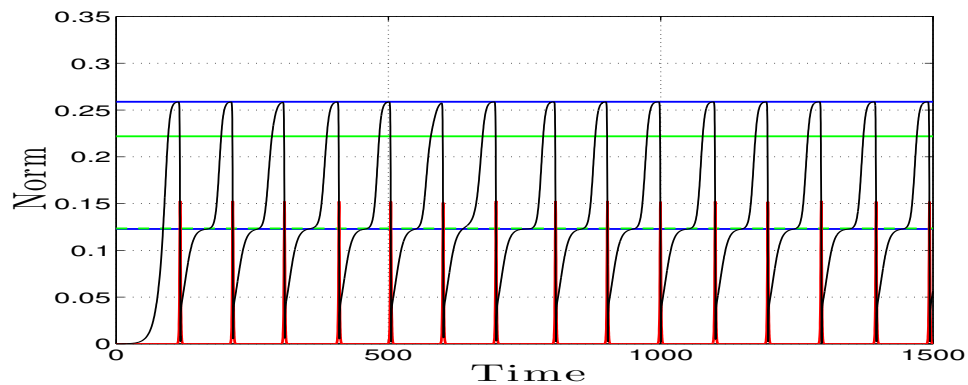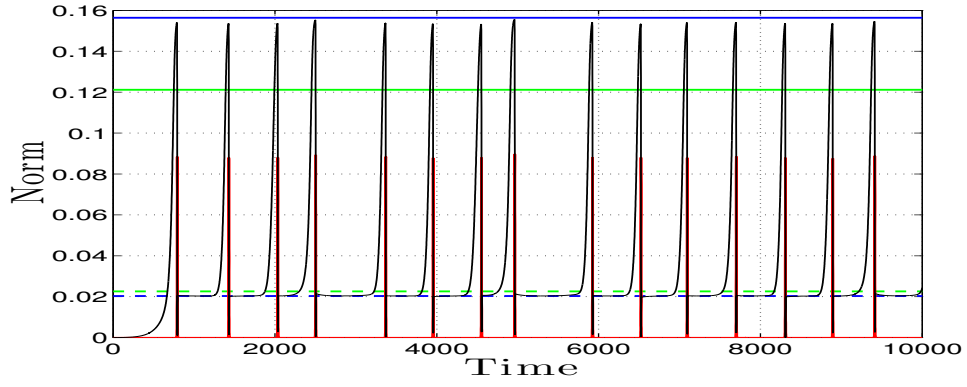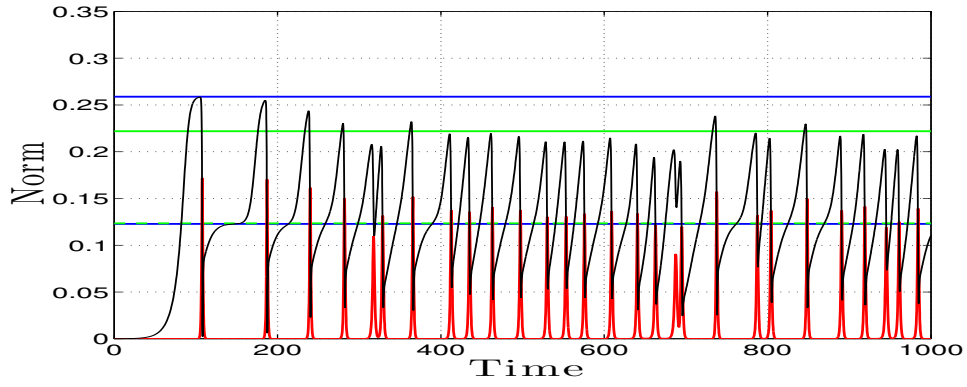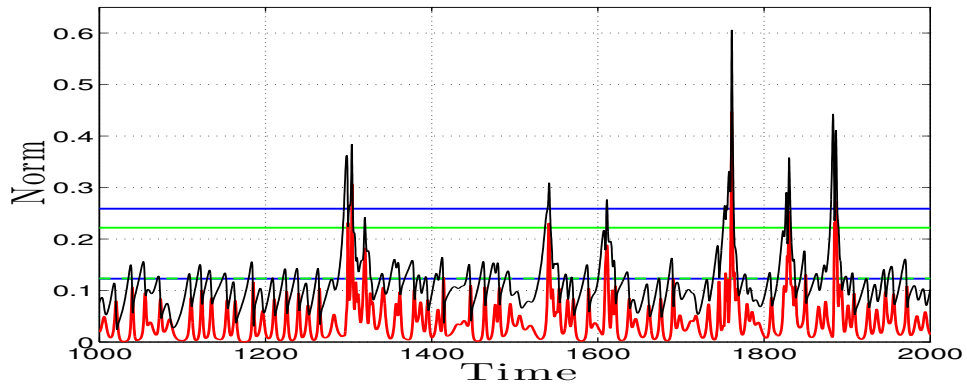Figure 25: Time series for $\mu_1 = -0.5, \mu_2 = 0.1$, $c = 0.04$. Same color code as in Fig. 17.

31

8 Conclusion

Intermittent dynamics near onset of convection has been analyzed for Rayleigh-Bénard type problems in a spherical shell. Here intermittency is closely linked to the existence of robust heteroclinic connections between bifurcated steady-states, robustness being understood as persistence against perturbative terms in the equations, which keep the spherical symmetry of the problem. When the heteroclinic connections close up in a cycle, nearby dynamics exhibit intermittent behavior with long periods of time passed near the steady-states followed by quick jumps to the next steady-state. A necessary condition for the occurrence of these heteroclinic cycles in problems with spherical symmetry is that spherical modes with degrees ℓ and $\ell + 1$ compete for destabilization of the initial state of rest. Here we have analyzed the case $\ell = 3$, corresponding to an aspect ratio of the order of 0.45.

We have shown that robust "generalized" heteroclinic cycles do indeed exist in certain range of parameters for this problem. These invariant sets connect steady-states with octahedral patterns, and secondary connections do also exist with axisymmetric patterns. These steady-states are pure 4-modes. In certain cases, connections with mixed-mode steady-states do also exist.

We have not rigorously studied the asymptotic stability of the generalized heteroclinic cycles. A complete analysis was performed earlier in the case $\ell = 1$, which was already quite involved [18]. Instead, we performed a numerical exploration of the dynamics on the center manifold, for parameter ranges where the heteroclinic cycles are expected to exist near onset of convection.
We did not find clearly stable heteroclinic cycles for the cubic approximation of the system reduced to the center manifold. Nevertheless we have numerically shown that dynamics mimicking heteroclinic cycles do indeed exist in small ranges of parameter values. It shows relatively long periods of quasi-static regime with octahedral or axisymmetric patterns, followed by fast switches to other quasi-steady states of the same kind. Some of these dynamics correspond to trajectories which clearly follow generalized heteroclinic cycles, which therefore are "nearly stable". Others are less clearly driven by the heteroclinic cycles, but nevertheless occur through scenarios which are related to the "heteroclinic" mechanism.

The asymptotic stability of these generalized heteroclinic cycles is a pending question. By suitably choosing coefficient values of the normal form (9), which however are not compatible with the physical problem of onset of convection, conditions can be found at which it is numerically observed that the dynamics seemingly converge to generalized heteroclinic cycles. Three videos of the time evolution of such patterns are posted in `http://math.unice.fr/~chossat`, corresponding respectively to generalized heteroclinic cycles of type I(i), I(iii) and II. In these cases the eigenvalues at each steady-state in the cycle satisfy strong contraction versus weak expansion. However a rigorous analysis of these cases has not yet been undertaken.

Another question is the range of validity of this analysis. It is probably quite narrow. Direct simulations would help to evaluate this range.
Finally, let us mention the problem of adding a small rotation to the domain on this dynamics, which breaks spherical symmetry and can also be analyzed using center manifold reduction.

References

[1] E. Doedel *et al. AUTO 2000: Continuation and bifurcation software for ordinary differential equations (with HomCont)* (2001)Tech. Rep. (Caltech, 2001).

[2] S. Chandrasekhar. *Hydrodynamic and Hydromagnetic Stability*, Dover, New-York, (1961).

[3] W.-G. Früh. *Using magnetic fluids to simulate convection in a central force field in the laboratory*, Nonlin. Processes Geophys., New-York, **12** (2005), 877-899.

[4] I. Yavorskaya, M. Fomina, N. I. Balyaev, N. and Yu. *A simulation of central-symmetry convection in microgravity conditions*, Acta Astronautica, **11** (1984), 179-180.

[5] A. Barletta and D.A. Nield. *Effect of pressure work and viscous dissipation in the analysis of the Rayleigh-Bénard problem*, International Journal of Heat and Mass Transfer, **52**(13-14) (2009), 3279 - 3289.

[6] ID. Puigjaner, J. Herrero, C. Sim and F. Giralt. *From steady solutions to chaotic flows in a Rayleigh-Bénard problem at moderate Rayleigh numbers*, Physica D, **240**(11) (2011), 920-934.

[7] V. Travnikov, Ch. Egbers and R. Hollerbach. *et at al. The GeoFlow-Experiment on ISS (Part II): Numerical simulation*, J. Adv. Space Res., **32** (2003), 184-190.

[8] P. Beltrame, and Ch. Egbers and R. Hollerbach. *et at al. The GeoFlow-Experiment on ISS (Part III): Bifurcation Analysis*, J. Adv. Space Res., **32** (2003), 191-197.

[9] Ch. Egbers *et at al. The GeoFlow-Experiment on ISS (Part I): Experimental preparation and design of laboratory testing hardware*, J. Adv. Space Res., **32** (2003), 171-183.

[10] P. Chossat. *Bifurcation and stability of convective flows in a rotating or not rotating spherical shell*, S.I.A.M. J. Appl. Math., 37, 3 (1979), p. 624-647.

[11] P. Ashwin, P. Chossat. *Attractors for robust heteroclinic cycles with continua of connections*, J. of Nonlinear Sc. **8** (1998), 103-130.

[12] P. Chossat. *The bifurcation of heteroclinic cycles in systems of hydrodynamical type*, Journal on Continuous, Discrete and Impulsive System, **8a**, 4 (2001), 575-590.

[13] D. Armbruster, P. Chossat. *Heteroclinic orbits in a spherically invariant system*, Physica D 50 (1991), 155-176.

[14] P. Beltrame, V. Travnikov, M. Gellert and C. Egbers. *GEOFLOW: simulation of convection in a spherical shell under central force field in terrestrial and microgravity environments*, Nonlinear Processes in Geophysics, **13**, (2006), 413-423.

[15] P. Chossat, F. Guyard. *Heteroclinic cycles in bifurcation problems with O(3) symmetry*, J. of Nonlinear Science 6 (1996), 201-238.

[16] P. Beltrame, C. Egbers. *The (3,4) Mode Interaction in the GeoFlow Framework*, Proc. Appl. Math. and Mechanics (2004), 474-475.

[17] A. Vanderbauwhede and G. Iooss. *Center Manifold Thoery in Infinite Dimension,* John Wiley & sons and B.G. Teubner, London, Vol. 1 New series, 1992, 125-163.

[18] P. Chossat, F. Guyard, R. Lauterbach. *Generalized heteroclinic cycles in spherically invariant systems and their perturbations*, J. of Nonlinear Science **9** (1999), 479-524.

[19] P. Chossat, R. Lauterbach, I. Melbourne. *Steady-State bifurcation with O(3)-symmetry*, Archive for Rat. Mech. Anal. 113 (1990), 313-376.

[20] P. Chossat, R. Lauterbach. *Equivariant bifurcation theory and its applications*, Advanced Series in Nonlinear Dynamics 15, World Scientific, Singapur (2000).

[21] C. Egbers, W. Beyer, A. Bonhage, R. Hollerbach, P. Beltrame. *The geoflow-experiment on ISS (part I): Experimental preparation and design of laboratory testing hardware.* Advances in Space Research, **32**, 2 (2003) 171-180.

[22] M. Field. *Equivariant bifurcation theory and symmetry breaking*, J. Dyn. Diff. Equat. **1**, 1989, 369-421.

[23] R. Friedrich and H. Haken. *Static, wavelike and chaotic thermal convection in spherical geometries*, Phys. Rev. A, **34**, (1986) 2100–2120.

[24] C. Geiger, G. Dangelmayr, J.D. Rodriguez and W. Guttinger. *Symmetry breaking bifurcations in spherical Benard convection. I: Results from singularity theory.* Fields Institute Communications Vol. 5, American Mathematical Society, Providence, RI, 1993, 225–237.

[25] M. Gellert, P. Beltrame and C. Egbers. *The GeoFlow experiment - spherical Rayleigh-Bénard convection under the influence of an artificial central force field.* Journal of Physics: Conference Series 14 (2005) 157-161.

[26] M. Golubitsky, I. Stewart, D. Schaeffer. *Singularities and groups in bifurcation theory* Vol. 2, Appl. Math. Sci. **69**, Springer Verlag (1988).

[27] M. Krupa and I. Melbourne. *Asymptotic stability of heteroclinic cycles in systems with symmetry.* Erg. Th. Dyn. Sys. 15 (1995), 121-147

[28] J.D. Rodriguez, C. Geiger, G. Dangelmayr and W. Guttinger. *Symmetry breaking bifurcations in spherical Benard convection. II: Numerical results.* Fields Institute Communications Vol. 5, American Mathematical Society, Providence, RI (1996), 239–253.

A   The lattice of isotropies for the $3, 4$ mode interaction

Numbers on the left indicate the dimension of corresponding fixed point subspaces.
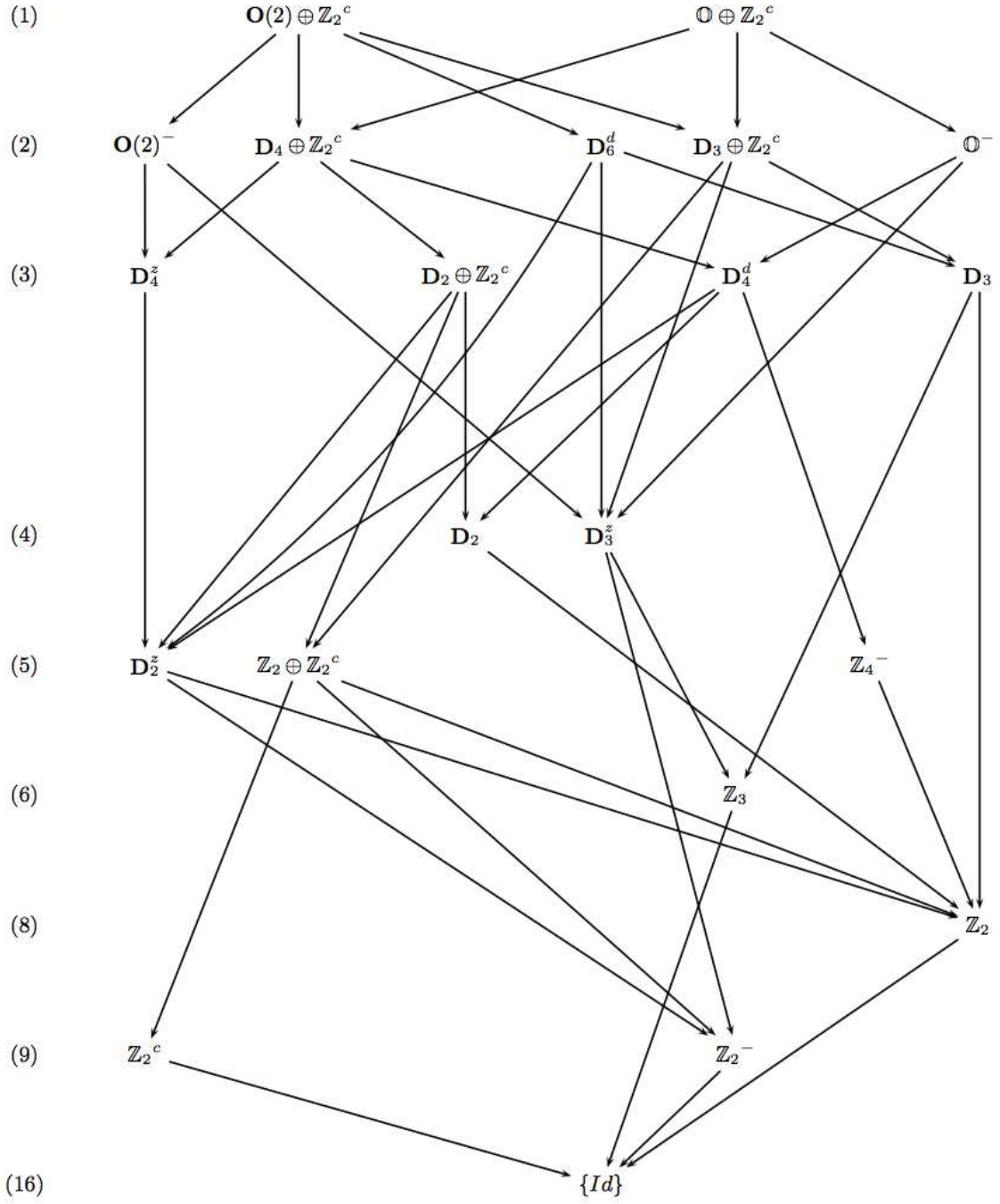
B The quadratic and cubic equivariant terms in (9)

In the tables below we display the coefficients of quadratic and cubic terms in equations (9a) and (9b). Conventions are as follows: Number m in the "Equation" column indicates the index of the component along the spherical harmonic Y_ℓ^m, with $\ell = 3$ or 4 depending on the map under consideration. We list only the coefficients for the components with $m = 0, \cdots, +\ell$, since the components for negative m are obtained from the ones with positive m according to the rule $Y_\ell^{-m} = (-1)^m \overline{Y}_\ell^m$. The numbers in parenthesis in the column "terms" indicate the indices of the corresponding terms with the following convention: (i, j) for the quadratic terms $x_i y_j$ ($-3 \leq i \leq 3$, $-4 \leq j \leq 4$), (ij) for the terms $x_i x_j$ ($-3 \leq i \leq j \leq 3$) or $y_i y_j$ ($-4 \leq i \leq j \leq 4$), and (ijk) for the cubic terms $y_i y_j y_k$ ($-4 \leq i \leq j \leq k \leq 4$).

Equation	Term	Coefficient	Equation	Term	Coefficient
3	$(0,3)$	$-3\sqrt{7}$	2	$(-2,4)$	$\sqrt{70}$
	$(-1,4)$	$\sqrt{42}$		$(-1,3)$	$-\sqrt{14}$
	$(1,2)$	$3\sqrt{6}$		$(0,2)$	$-\sqrt{3}$
	$(2,1)$	$-\sqrt{30}$		$(1,1)$	$4\sqrt{2}$
	$(3,0)$	3		$(2,0)$	-7
				$(3,-1)$	$\sqrt{30}$
1	$(-3,4)$	$\sqrt{42}$	0	$(-3,3)$	$\sqrt{7}$
	$(-2,3)$	$\sqrt{14}$		$(-2,2)$	$-\sqrt{3}$
	$(-1,2)$	$-2\sqrt{10}$		$(-1,1)$	$-\sqrt{15}$
	$(0,1)$	$\sqrt{15}$		$(0,0)$	6
	$(1,0)$	1		$(1,-1)$	$-\sqrt{15}$
	$(2,-1)$	$-4\sqrt{2}$		$(2,-2)$	$-\sqrt{3}$
	$(3,-2)$	$3\sqrt{6}$		$(3,-3)$	$\sqrt{7}$

Table 4: Coefficients for the quadratic "mixed" $\ell = 3$ map $Q^{(1)}$

Equation	Term	Coefficient	Equation	Term	Coefficient
4	(13)	$-\sqrt{42}$	3	(03)	$3\sqrt{7}$
	(22)	$\sqrt{70}/2$		(12)	$\sqrt{14}$
2	(02)	$-\sqrt{3}$	1	(01)	$\sqrt{15}$
	(11)	$\sqrt{10}$		(-12)	$-4\sqrt{2}$
	(-13)	$-6\sqrt{3}$		(-23)	$-\sqrt{30}$
0	(00)	3			
	(-11)	-1			
	(-22)	-7			
	(-33)	-3			

Table 5: Coefficients for the quadratic "mixed" $\ell = 4$ map $Q^{(2)}$

Equation	Term	Coefficient	Equation	Term	Coefficient
4	(04)	14	3	(−14)	$7\sqrt{10}$
	(13)	$-7\sqrt{10}$		(03)	−21
	(22)	$3\sqrt{70}/2$		(12)	$\sqrt{70}$
2	(−24)	$3\sqrt{70}$	1	(−34)	$7\sqrt{10}$
	(−13)	$-\sqrt{70}$		(−23)	$\sqrt{70}$
	(02)	−11		(−12)	$-6\sqrt{10}$
	(11)	$3\sqrt{10}$		(01)	9
0	(00)	9			
	(−11)	−9			
	(−22)	−11			
	(−33)	21			
	(−44)	14			

Table 6: Coefficients for the quadratic "pure" $\ell = 4$ map $Q^{(3)}$

Equation	Term	Coefficient	Equation	Term	Coefficient
3	(−333)	−45	2	(−323)	−45
	(−223)	45		(−213)	$10\sqrt{15}$
	(−113)	−15		(−222)	20
	(−122)	$-5\sqrt{15}$		(−103)	$-15\sqrt{2}$
	(003)	0		(−112)	−35
	(012)	$15\sqrt{2}$		(002)	30
	(111)	$-2\sqrt{15}$		(011)	$\sqrt{30}$
1	(−313)	−15	0	(−303)	0
	(−322)	$-5\sqrt{15}$		(−312)	$-15\sqrt{2}$
	(−203)	$-15\sqrt{2}$		(−202)	60
	(−212)	35		(−211)	$-5\sqrt{6}$
	(−1 − 13)	$-6\sqrt{15}$		(−101)	−36
	(−102)	$2\sqrt{30}$		(000)	18
	(−111)	−41			
	(001)	18			

Table 7: Coefficients for the cubic "pure" $\ell = 3$ map $C^{(1)}$

Equation	Term	Coefficient	Equation	Term	Coefficient
4	(-444)	$30/7$	3	(-434)	$30/7$
	(-334)	$-30/7$		(-324)	$-5\sqrt{7}/2$
	(-224)	$-5/7$		(-333)	$5/56$
	(-233)	$5\sqrt{7}/4$		(-214)	$15/4$
	(-114)	$45/14$		(-223)	$135/56$
	(-123)	$-15/4$		(-104)	$-\sqrt{10}/4$
	(004)	$-13/7$		(-113)	$-65/56$
	(013)	$\sqrt{10}/4$		(-122)	$-45\sqrt{7}/56$
	(022)	$3\sqrt{5/14}$		(003)	$-17/28$
	(112)	$-5\sqrt{7}/14$		(012)	$23/4\sqrt{5/14}$
				(111)	$-15/28\sqrt{7}$
2	(-424)	$-5/7$	1	(-414)	$-45/14$
	(-433)	$5\sqrt{7}/4$		(-423)	$15/4$
	(-314)	$-15/4$		(-304)	$-\sqrt{10}/4$
	(-323)	$-135/56$		(-313)	$-65/56$
	(-204)	$3\sqrt{10/7}$		(-322)	$-45\sqrt{7}/56$
	(-213)	$45\sqrt{7}/28$		$(-2-14)$	$5\sqrt{7}/7$
	(-222)	0		(-203)	$23/4\sqrt{5/14}$
	$(-1-14)$	$-10\sqrt{7}/28$		(-212)	$15/8$
	(-103)	$-23/4\sqrt{5/14}$		$(-1-13)$	$-45\sqrt{7}/28$
	(-112)	$-15/8$		(-102)	$3\sqrt{10}/4$
	(002)	$7/2$		(-111)	$-25/8$
	(011)	$-3\sqrt{10}/8$		(001)	1
0	(-404)	$-26/7$			
	(-413)	$\sqrt{10}/4$			
	(-422)	$3\sqrt{70}/14$			
	$(-3-14)$	$\sqrt{10}/4$			
	(-303)	$17/14$			
	(-312)	$-23/4\sqrt{5/14}$			
	$(-2-24)$	$3\sqrt{5/14}$			
	$(-2-13)$	$-23/4\sqrt{5/14}$			
	(-202)	7			
	(-211)	$3\sqrt{10}/8$			
	$(-1-12)$	$3\sqrt{10}/8$			
	(-101)	-2			
	(000)	1			

Table 8: Coefficients for the cubic "pure" $\ell = 4$ map $C^{(2)}$

C Computation of the coefficients in Equations (9)

The relation between the first terms of the Taylor series expansion (8) and the associated evolution problem (6) are shown in [15]:

$$R^1_{1,0}(U) = P_0 L_1 \tag{20}$$

$$R^1_{0,1}(U) = P_0 L_2 \tag{21}$$

$$R^2_{0,0}(U,U) = P_0 M(U,U) \tag{22}$$

$$R^3_{0,0}(U,U,U) = -2P_0 M(U, SM(U,U)) \tag{23}$$

S designates the pseudo-inverse of L_0 defined as the inverse of the restriction of L_0 onto the kernel of P_0. If $(\zeta^{(\ell)}_m)_{m=-\ell...\ell}$ is a base of V_ℓ, the P_0 projection reads:

$$P_0 Z = \Sigma^3_{m=-3} \left\langle Z, \zeta^{*(3)}_m \right\rangle + \Sigma^4_{n=-4} \left\langle Z, \zeta^{*(4)}_m \right\rangle \tag{24}$$

where $(\zeta^{*(\ell)}_m)$ is the adjoint vector. P_0 can be defined using the scalar product: Then the bifurcation parameters μ_1 and μ_2 are related to physical parameters by:

$$\begin{cases} \mu_1 = \left\langle L_1 \zeta^{(3)}_0, \zeta^{*(3)}_0 \right\rangle \tilde{\lambda} + \left\langle L_2 \zeta^{(3)}_0, \zeta^{*(3)}_0 \right\rangle \tilde{\eta} \\ \mu_2 = \left\langle L_1 \zeta^{(4)}_0, \zeta^{*(4)}_0 \right\rangle \tilde{\lambda} + \left\langle L_2 \zeta^{(4)}_0, \zeta^{*(4)}_0 \right\rangle \tilde{\eta} \end{cases} \tag{25}$$

In order to find the quadratic coefficients, we have to identify one term of the quadratic polynomials (see Tab 6) with the terms of the right side of the relation (22):

$$b = \frac{1}{3} \left\langle M\left(\zeta^{(3)}_0, \zeta^{(3)}_0\right), \zeta^{*(4)}_0 \right\rangle$$

$$\beta = \frac{1}{6} \left\langle M\left(\zeta^{(3)}_0, \zeta^{(4)}_0\right), \zeta^{*(3)}_0 \right\rangle$$

$$c = \frac{1}{9} \left\langle M\left(\zeta^{(4)}_0, \zeta^{(4)}_0\right), \zeta^{*(4)}_0 \right\rangle$$

The same procedure is applied for the cubic coefficients. However, there is two independent cubic polynomials for each representation ℓ. Therefore, we need to identify two terms of the polynomials in order to get two linear indepedent equations. We chose the terms (000) and (002) of the cubic invariant polynomials. The coefficient in front of the (000), resp. (002), term is noted $c^{(i)}_0$, resp. $c^{(i)}_2$, for the $C^{(i)}$ invariant polynomial. We obtain the following expressions:

$$c^{(1)}_0 = -2 \left\langle M\left(\zeta^{(3)}_0, SM\left(\zeta^{(3)}_0, \zeta^{(3)}_0\right)\right), \zeta^{*(3)}_0 \right\rangle$$

$$c^{(1)}_2 = -2 \left\langle M\left(\zeta^{(3)}_2, SM\left(\zeta^{(3)}_0, \zeta^{(3)}_0\right)\right), \zeta^{*(3)}_2 \right\rangle$$
$$-4 \left\langle M\left(\zeta^{(3)}_0, SM\left(\zeta^{(3)}_0, \zeta^{(3)}_2\right)\right), \zeta^{*(3)}_2 \right\rangle$$

$$c^{(2)}_0 = -2 \left\langle M\left(\zeta^{(4)}_0, SM\left(\zeta^{(4)}_0, \zeta^{(4)}_0\right)\right), \zeta^{*(4)}_0 \right\rangle$$

$$c^{(2)}_2 = -2 \left\langle M\left(\zeta^{(4)}_2, SM\left(\zeta^{(4)}_0, \zeta^{(4)}_0\right)\right), \zeta^{*(4)}_2 \right\rangle$$
$$-4 \left\langle M\left(\zeta^{(4)}_0, SM\left(\zeta^{(4)}_0, \zeta^{(4)}_2\right)\right), \zeta^{*(4)}_2 \right\rangle$$

After identification with the sum of equivariant polynomials and solving the linear systems, the bifurcation coefficients are given by:

$$\gamma_1 = \frac{1}{2}\left(5c_0^{(1)} - 3c_2^{(1)}\right) \tag{26}$$

$$\gamma_2 = \frac{1}{12}\left(-c_0^{(1)} + c_2^{(1)}\right) \tag{27}$$

$$d_1 = \frac{1}{5}\left(7c_0^{(2)} - 2c_2^{(2)}\right) \tag{28}$$

$$d_2 = \frac{2}{5}\left(-c_0^{(2)} + c_2^{(2)}\right) \tag{29}$$

D   Eigenvalues along the heteroclinic connections in generalized heteroclinic cycles of type I

In the diagrams of Theorem 1 we indicated which eigenvalues, at each equilibrium in the generalized heteroclinic cycle, give the rate of expansion or contraction along the connections in the cycle. Expressions for the eigenvalues are given in Tables 2 and 3. We display in Table 9 these eigenvalues in the different cases where type I generalized heteroclinic cycles appear to drive the dynamics in the numerical simulations of Section 7.

A criterion for the stability of simple heteroclinic cycles (cycles with heteroclinic saddle-sink connections occuring in invariant planes only) is that the ratio of the product of positive (expanding) eigenvalues by the product of the absolute value of negative (contracting) eigenvalues be less than 1 [27]. We observe that this criterion is satisfied in all cases displayed in the table, although the generalized heteroclinic cycles do not seem to be asymptotically stable in the time integrations and with the initial conditions which have been used.

	$c=0.004, \mu_1 = 0.12,\ \mu_2 = 0.002$		$c=0.04, \mu_1 = -1.17, \mu_2 = 0.1$		$c=0.04, \mu_1 = -0.61, \mu_2 = 0.01$	
	α_+	α_-	α_+	α_-	α_+	α_-
σ_2^α	0.6068 ;	$-$	0.3834 ;	$-$	0.2381 ;	$-$
λ_2^α	-0.09456 ; 0.004189		-0.2301 ; 0.08246		-0.1126 ; 0.01753	
λ_3^α	-0.1172 ; 0.006347		-0.2325 ; 0.1585		-0.1353 ; 0.02747	
λ_4^α	0.03391 ; -0.001021		0.1044 ; -0.006122		0.04212 ; -0.003897	
	β_+	β_-	β_+	β_-		
σ_0^β	0.1817 ; -0.29706		1.202 ; -2.296		0.8229 ; -0.7964	
σ_2^β	-0.0697;	$-$	-0.775 ;	$-$	-0.3712 ;	$-$
λ_2^β	-0.002547 ; $5.944 \cdot 10^{-5}$		-0.1744 ; 0.01607		-0.08252 ; 0.005625	
λ_3^β	-0.004408 ; 0.002228		-0.3401 ; 0.1448		-0.1997 ; 0.02471	

Table 9: Eigenvalues for the type-I heteroclinic cycles in some cases.